Formica exsecta increases heterogeneity in the grassland ecosystem Alp Stabelchod in the Swiss National Park

Aline Morger; 15-934-748 **03 February 2022**

Master's Degree program in Environmental Sciences, Department of Environmental System Science, ETH Zürich

Supervisor: **PD Dr. Anita Risch**. Swiss Federal Institute for Forest, Snow and Landscape Research (WSL), Community Ecology

Co-Supervisors: **Dr. Martin Schütz.** Swiss Federal Institute for Forest, Snow and Landscape Research (WSL), Community Ecology

Christian Rossi. University of Zurich, Swiss Federal Institute for Forest, Snow and Landscape Research (WSL) and Swiss National Park (SNP), Geoinformation

WSL parc naziunal svizzer DUSYS ETH Eidgenössische Technische Hochschule Zürich Swiss Federal Institute of Technology Zurich

ETH

Eidgenössische Technische Hochschule Zürich
Swiss Federal Institute of Technology Zurich

Declaration of originality

The signed declaration of originality is a component of every semester paper, Bachelor's thesis, Master's thesis and any other degree paper undertaken during the course of studies, including the respective electronic versions.

Lecturers may also require a declaration of originality for other written papers compiled for their courses.

I hereby confirm that I am the sole author of the written work here enclosed and that I have compiled it in my own words. Parts excepted are corrections of form and content by the supervisor.

Title of work (in block letters):

Formica exsecta increases heterogeneity in the grassland ecosystem Alp Stabelchod in the Swiss National Park

Authored by (in block letters):

For papers written by groups the names of all authors are required.

Name(s):	First name(s):
Morger	Aline Julia

With my signature I confirm that

- – I have committed none of the forms of plagiarism described in the 'Citation etiquette' information sheet
- – I have documented all methods, data and processes truthfully.
- – I have not manipulated any data.
- – I have mentioned all persons who were significant facilitators of the work.

I am aware that the work may be screened electronically for plagiarism.

Place, date	Signature(s)
Zurich, 02.02.22	

For papers written by groups the names of all authors are required. Their signatures collectively guarantee the entire content of the written paper

Abstract

Ants are important ecosystem engineers who affect soil properties, the flow of energy and nutrients across ecosystems, and greatly impact the maintenance of ecosystem heterogeneity. However, there is still a lack of knowledge regarding the role of ants in temperate grasslands and larger scale information about nest densities and patterns is rarely available. In this study I quantified the nest mounds of a *Formica exsecta* Nyl. supercolony on a subalpine grassland in the Swiss National Park (SNP), using an unmanned-aerial-vehicle-based thermal infrared camera. I measured and compared total nitrogen (N) and carbon (C) concentrations of the soil and the vegetation on and off ant mounds, and calculated the contribution of the ant mounds to the grassland's N and C pools. The number of *F. exsecta* mounds on the grassland has increased to more than 1600 mounds over the past ten years. Although the ant mounds only contributed less than 1% to the soil N and C pools on Alp Stabelchod, *F. exsecta* increased the heterogeneity across the grassland. Ant mounds were characterized by higher soil temperature. Significantly lower soil bulk densities were paralleled by higher total soil N and C concentrations compared to the surrounding grassland. Additionally, the vegetation growing on ant mounds contained significantly higher N and lower C concentrations compared to the vegetation growing off the ant mounds. Heterogeneity was enhanced at a local, but also at an ecosystem level due to the heterogenous distribution of the ant mounds. This increased heterogeneity possibly affects other trophic levels, for example, plant species composition, invertebrate or microbial decomposers or large primary consumers such as red deer.

Acknowledgments

I would like to express my special thanks to my supervisor Anita Risch and my co-supervisors Martin Schütz and Christian Rossi for their great support during this Master's thesis. Through their valuable input, detailed feedback and support with any questions that arose, I was able to learn a lot during the process. In addition, the lively exchange via Zoom or during the fieldwork was always fun and allowed me to learn a lot that went beyond the thesis itself. I would also like to thank Samuel Wiesmann for his contribution to the planning and implementation of the drone flight, Sonja Wipf and the entire SNP for providing the great accommodation in the Labor II Fuorn, for the permission of the research activity and access to the research sites. Also, to all the people at WSL who introduced me to the various methods and research equipment, including Marco Walser and Janka Bollenbach. To Chiara Vanetta for her great support with the statistics. I would also like to acknowledge Yongyong Zhang and Johanna Ertle for their support during the fieldwork, Valentin Moser and Carol Resch for sharing their experiences with writing a Master's thesis in general, Roman Zürcher for proofreading, and to all the people who I crossed paths with during these six months who made this time a unique and memorable experience.

Contents

Abstract iii

Acknowledgments iv

Contents v

List of Figures vii

Appendix Figures viii

List of Tables viii

1 Introduction 1

1.1 Research Questions 3

2 Methods 4

2.1 Study site and study organism 4

2.2 Study design 5

2.3 Soil sampling 5

2.4 Vegetation sampling 6

2.5 Counting ant mounds using remote sensing 7

2.6 Training independent validation of mound counts 8

2.7 Determination of mound diameter and height 8

2.8 Calculation of C and N pools 9

2.9 Statistical analyses 10

3 Results 12

3.1 Remote Sensing 12

3.1.1 Image Processing and visual inspection 12

3.1.2 Detecting *Formica exsecta* mounds using deep learning 12

3.2 Temporal ant mound patterns 13

3.3 Soil and vegetation properties 15

3.3.1 Soil C and N concentrations 15

3.3.2 Soil bulk density 16

3.3.3 Vegetation C and N concentrations 17

3.4 C an N pools 17
3.4.1 Mound heights and diameters 17
3.4.2 Contribution of ant mounds to the overall C and N pool 18
4 Discussion 19
4.1 Detection of ant mounds using remote sensing 19
4.2 Temporal and spatial patterns in the occurrence of *F. exsecta* mounds 20
4.3 C and N accumulation in *F. exsecta* mounds 23
4.4 Grassland C and N pools 24
5 Conclusions 26
Bibliography 27
Appendix 32
A.1 Temperature curve and differences between ant hill and surroundings 32
A.2 Quality Report 35
A.3 Optimized Hot Spot Analysis 44
A.4 Diameter distribution of ant mounds on Alp Stabelchod 45

List of Figures

Figure 1: Schematic illustration of the 268 cells (20 m x 20 m) covering the entire grassland Alp Stabelchod. 20 grid cells containing at least one ant mound were randomly selected and used for soil and vegetation sampling. 12 additional cells were randomly selected for mound count validation. 5

Figure 2: Schematic illustration of the sampling method. Soil cores of 10 cm height and 5 cm diameter were extracted on the mound, directly under the mound and at a distance of 2 meters from the mound center. The vegetation from an area of 10 cm x 10 cm was cut on the mound edge and at a distance of 2 meters from the mound center. 6

Figure 3: Schematic illustration of the classification of the electromagnetic spectrum into bands. The figure is adapted from PROTHERM (retrieved on January 15 from *https://www.pro-therm.com/infrared_basics.php*). The sensor used in this study is sensitive for the long wave region of infrared. 8

Figure 4: The formulas used for the calculation of volumes and total nutrient content of the different sampling locations *(aboveground and belowground mound, off mound)* are given. A schematic illustration visualizes how the different parameters were collected. The average bulk densities (BD_i) and nutrient concentrations (NC_i) were calculated for each sampling location. Radii R_1 and R_2 were calculated by overlaying a *Minimal Bounding Rectangle (dotted rectangle)* in ArcGIS Pro 2.7.0 and height h was derived from the average radius via fitting a GAM on diameter and height data available. The variable x corresponds to the sampling depth extracted with the stainless-steel corer. 10

Figure 5: The orthorectified and georeferenced thermal layer of Alp Stabelchod serves as an overview (A). More detailed extracts are given in B and C with the corresponding model outputs where the detected mounds are marked in red. In the thermal image *F. exsecta* mounds appear as spots of high temperature (white), surrounded by cooler vegetation (grey). 11

Figure 6: Linear regression (blue) between the number of *F. exsecta* mounds observed by field survey (x-axis) and the number of mounds predicted by the Deep Learning model (y-axis) at a classification threshold of 50%. The red dashed line corresponds to a 1:1 ratio. RMSE, R-squared and p-values are given in the plot. 13

Figure 7: Grid-wise count data of *F. exsecta* mounds from the years A. 1998, B. 2007 and C. 2021. In white colored fields, no mounds were detected, darker colors indicate higher counts. 14

Figure 8: Grid-wise count differences of *F. exsecta* mounds between the timepoints (A.) 2007 – 1998 and (B.) 2021 – 2007. White cells indicate no change. Orange to red cells indicate a mound reduction, fair green to dark green an increase between the two respective time points. 14

Figure 9: Relationships between soil N concentration [%] from (A) aboveground (y-axis) versus belowground (x-axis) parts of ant mounds, (B) aboveground parts of mounds (y-axis) versus off the mounds soil (x-axis) and (C) belowground parts of ant mounds (y-axis) versus off the mounds soil (x-axis). The red dashed line corresponds to the 1:1 ratio. 15

Figure 10: Relationships between soil C concentration [%] from (A) aboveground (y-axis) versus belowground (x-axis) parts of ant mounds, (B) aboveground parts of mounds (y-axis) versus off the

mounds soil (x-axis) and (C) belowground parts of ant mounds (y-axis) versus off the mounds soil (x-axis). The red dashed line corresponds to the 1:1 ratio. 16

Figure 11: Soil bulk density [kg m^{-3}] is plotted for the three sampling locations: The surrounding reference soil, the soil sampled from belowground part of the ant mounds and the soil sampled from the aboveground part. 16

Figure 12: Relationships between vegetation sampled on ant mounds (y-axis) versus off mounds (x-axis) regarding (A) nitrogen concentration [%] and (B) carbon concentration [%]. The red dashed line corresponds to the 1:1 ratio. 17

Figure 13: Univariate GAM fitted to explore the relationship between the average diameter (x-axis) and height of an ant mound (y-axis): Height ~ s(Average Diameter), (n = 2309). The model was highly significant for the smooth term ($p < 0.001$) and approximately cubic (estimated degrees of freedom = 3.34). 18

Appendix Figures

Appendix Figure 1: Temperature course at 10 cm above ground (blue), on the surface (orange) and at 10 cm below ground (grey) of a *F. exsecta* mound. 32

Appendix Figure 2: Temperature course at 10 cm above ground (blue), on the surface (orange) and at 10 cm below ground (grey) measured at 2 m distance of the *F. exsecta* mound. 33

Appendix Figure 3: Temperature difference between logger located on *F. exsecta* mound and at 2 meters distance of the mound measured at 10 cm above ground (blue), on the surface (orange) and at 10 cm below ground (grey). 34

Appendix Figure 4: Optimized Hotspot Analysis (Spatial Statistics Toolbox; ArcGIS Pro 2.7.0) for the year 1998 (A), 2007 (B) and 2021 (C). This tool identifies statistically significant spatial clusters with high values (hot spots; red) and with low values (cold spots; blue) of mound counts. The size of the hot and cold spots varies over the years but the location remains to stay relatively stable. 44

Appendix Figure 5: *F. exsecta* mounds counted (y-axis) in nest diameter classes (x-axis) in the years 1998 (A.), 2007 (B.) and 2021 (C.) 45

List of Tables

Table 1: Total soil C and total soil N pools for the three sampling locations in relation to the grassland area they cover. 18

1 Introduction

Ants (Hymenoptera: Formicidae) are eusocial insects that have long been recognized for their key role in supporting ecological processes in most terrestrial ecosystems (Del Toro et al., 2012; Folgarait, 1998; Hölldobler & Wilson, 1990; Wills & Landis, 2018). Their effects on ecosystems are diverse and complex, as they can not only regulate ecosystems top-down as consumers, but also bottom-up as ecosystem engineers (Schumacher, 2010).

Through foraging, nest or mound building activities, ants are considered important regulators of animal and plant community structure (e.g. Del Toro et al., 2012; Wills & Landis, 2018). Ants have been reported to alter the abundance of other invertebrate species from all trophic levels, interfere with their behavior, and to affect plant species composition, diversity, abundance, and spatial heterogeneity (Konečná et al., 2021; Schütz et al., 2008; Escobar-Ramírez et al., 2012 and Prior et al., 2014 cited in Wills & Landis, 2018). In their role as ecosystem engineers, ants affect energy and nutrient flows across almost all types of terrestrial ecosystems (Wang et al., 2017) and greatly impact the maintenance of ecosystem heterogeneity (Jouquet et al., 2006) by altering the soil physical and chemical properties in the immediate surrounding of their nests. Altered soil physical properties include reduced soil density (Golichenkov et al., 2019), increased soil aggregate formation and porosity (Cammeraat & Risch, 2008; Drager et al., 2016), and altered soil infiltration rates (Cammeraat & Risch, 2008), whereas altered chemical soil properties such as carbon (C) or nutrient concentrations and dynamics, can significantly differ between ant nests and the surrounding soils (Del Toro et al., 2012; Lavelle et al., 2006; Schumacher, 2010; Wagner & Jones, 2006; Wu et al., 2010).

Even though the impacts of ant nests on soil properties have already been studied for a variety of different ecosystems and several ant species of high abundance or ecological importance, larger scale information about nest densities and patterns is rarely available but considered crucial to understand the impacts of ants on ecosystem level (Wu et al., 2013). Specifically, Wills & Landis (2018) concluded in their review, that there is still a lack of knowledge regarding the role of ants in temperate grasslands, especially on how they suppress pest, or affect soil C and nutrient cycling, microbial and plant community compositions.

With this study I aimed to contribute to the understanding of the role of ants in temperate grassland ecosystems and how they affect the distribution of soil C and soil nutrients. I therefore quantified nests of the mound-building ant species *Formica exsecta* Nyl. on a 11 ha large subalpine grassland in the Swiss National Park (SNP). I measured total nitrogen (N) and total C concentrations of the soil; in, below and off ant nests as well as in the vegetation on and off the same nests. I calculated the contribution of the nests to the overall C and N pools of the grassland and investigated whether ants accumulate C and N in their nests and thus increase the overall heterogeneity of the grassland.

The nests of the polydomous *F. exsecta* on Alp Stabelchod were already quantified in the years 1998 (unpublished) and 2007 (Schütz & Risch, 2013, 2014) via field survey by counting them manually. This approach is very time-consuming and therefore expensive. Field surveys also induce disturbance, which should be kept to a minimum in a protected area such as the SNP. Consequently, the nests of *F. exsecta* were only counted every 10 years despite an existing interest in higher temporal resolution of the data. I therefore decided to assess a different, potentially more widely applicable approach for counting ant nests. A method based on remote sensing combined with automated, computer-based nest detection could potentially reduce the amount of time and money spent and the level of disturbance created. It would, therefore, allow a shortening of observation time intervals in further research projects. Moreover, information about nest numbers and properties has to date been collected per cell (20 m x 20 m) of a grid spanning the entire grassland, making the identification of individual nests over time impossible. Remote sensing facilitates georeferencing of individual nests, thus enabling, for example, detailed observation of the changes in the dimensions of particular nests over time. To summarize: a method based on remote sensing would possibly allow studying nest dynamics with a higher temporal and spatial resolution in the future.

To the best of my knowledge, no study has so far examined the use of a thermal camera to detect *F.exsecta* mounds. The use of a remote sensing approach with or without thermal cameras to detect ant nests, however, has been examined in several studies, mainly focusing on the detection of mounds of ant species with adverse effects on humans, like the imported fire ant species *Solenopsis invicta* Buren and *Solenopsis richteri* Forel (Green et al., 1977; Klimetzek et al., 2021; Vogt, 2004b, 2004a; Vogt & Wallet, 2008; Wylie et al., 2021) or the red harvester ant *Pogonomyrex barbatus* (Dibner et al., 2015; Fletcher et al., 2007). A majority of these studies focused on sensors in the near-infrared (NIR)

spectrum, which was shown to have limitations (Song et al., 2020; Vogt & Oliver, 2006), In addition, in all these studies the sensors were mounted to aerial vehicles (planes) or satellite imagery (Fletcher et al. 2007, Vogt & Wallet 2008) which only provides coarse spatial resolution data. Furthermore, highly time-consuming photo-interpretive techniques were used (Green et al., 1977; Vogt, 2004b). Nevertheless, the increasing availability of sensors in the mid-infared (MIR) and low-infrared (LIR) spectrum have recently provided new opportunities for mound detection (Wylie et al., 2021). In particular, combining LIR sensors with unmanned aerial vehicles (UAV) (Song et al., 2020) allows collecting thermal data at high spatial resolutions.

Some characteristics make *F. exsecta*, in my perception, well suited for applying remote sensing. As the species cannot increase the temperature inside the nest via metabolic heat production, it particularly depends on direct insolation and is therefore mainly found in open grasslands and not in shaded woodlands (Seifert, 2000). The upper part of the nest, the mound, thus often works as solar collector (Kadochová & Frouz, 2013). While efficient ventilation systems can be used for thermoregulation inside the nest (Kadochová & Frouz, 2013), the mound surface of some ant species has been shown to reach temperatures of over 50°C during daytime, which is significantly higher than the one of the surrounding matrix (Streitberger & Fartmann, 2015). I therefore chose to investigate the use of an unmanned aerial vehicle (UAV) equipped with a thermal LIR camera for *F. exsecta* nest detection.

1.1 Research Questions

The main questions addressed with this study are the following:

- Is it possible to count *Formica exsecta* nests using a remote sensing approach?
- How has the ant mound density and overall mound volume changed over the past 20 years on Alp Stabelchod and are specific patterns visible?
- Do C and N concentrations of the soil and the vegetation differ on versus off the ant mounds?
- To what extent do ant mounds contribute to grassland C and N pools and their heterogeneity?

2 Methods

2.1 Study site and study organism

The study was conducted on Alp Stabelchod, a subalpine grassland located within the SNP. The SNP was founded in 1914 and is therefore the oldest national park in the Alps (IUCN, 2021). It is designated as Strict Nature Reserve (IUCN Management Category 1a), where human visitation, use and impacts are strictly controlled and limited to ensure protection of the conservation values (IUCN, 2021). The mean annual temperature since 1917, recorded at the parks weather station in Buffalora (1977 m), is 0.44°C ± 0.73 °C (mean ± SD) and the mean annual precipitation is 911 mm ± 166 mm (MeteoSchweiz, 2021). In the SNP, June represents the beginning of the growing season, which typically lasts until end of September. Alp Stabelchod is located at an elevation of 1950 m and has a uniform slope of 6° in southerly direction (Schütz et al., 2008). It was a summer pasture for cattle for about 500 years (Schorta, 1988 *cited in* Schütz et al., 2003) before agricultural use was stopped in 1918 (Schütz et al., 2003) after the foundation of the SNP.

Formica exsecta Nyl*,* is a mound building species which inhabits very different open or slightly shaded habitats (Seifert, 2018). *F.exsecta* can either live monogynous and monodomous or form polygynous and polydomous colonies (Pamilo, 1991). In Switzerland, the majority of colonies is generally polydomous and therefore polygynous (Kutter, 1977 *cited in* Maggini et al., 2002). On Alp Stabelchod we also find the polygynous and polydomous variety. This insect species is listed as “strongly endangered” in the Red List of endangered species in Switzerland, which corresponds to “vulnerable” in the IUCN Red List (Bundesamt für Umwelt Wald und Landschaft, 1994). Although it is probably the least endangered species from the subgenus *Coptoformica* in Central Europe, the populations of *F. exsecta* have dramatically declined since 1950 due to changes in forest management (i.e. afforestation of clearings and meadows, vanishing of coppice wood management) and intensified agriculture (Seifert, 2000).

2.2 Study design

The study took place from the beginning of June to end of July 2021. The open grassland of Alp Stabelchod comprises 10.7 ha and is covered with permanent corner posts of a grid of 268 cells (20 m x 20 m) that were installed by Achermann (2000), (Figure 1). The coordinates of 200 mounds evenly distributed across the grassland were recorded (Trimble GeoXR real-time kinematic GNSS; accuracy of < 0.10 m), and two perpendicular diameters, as well as the height of each mound were measured.

Mounds of *F. exsecta* were already counted twice on the grassland in 1998 and 2007 using grid cells to facilitated orientation (see Figure 2). In this current study I randomly selected 20 of these grid cells in which at least one mound was found. Within each cell I located the ant mound with a diameter of at least 20 cm closest to the cell center and marked it with a brush flag to ease monitoring. At each selected mound, the following samples were taken: (A) paired soil core samples from (1) the aboveground, (2) the belowground part of the mound and (3) two meters distance from the mound center, (B) paired samples of aboveground vegetation (1) on the mound as well as (2) at two meters distance from the mound center (Figure 2).

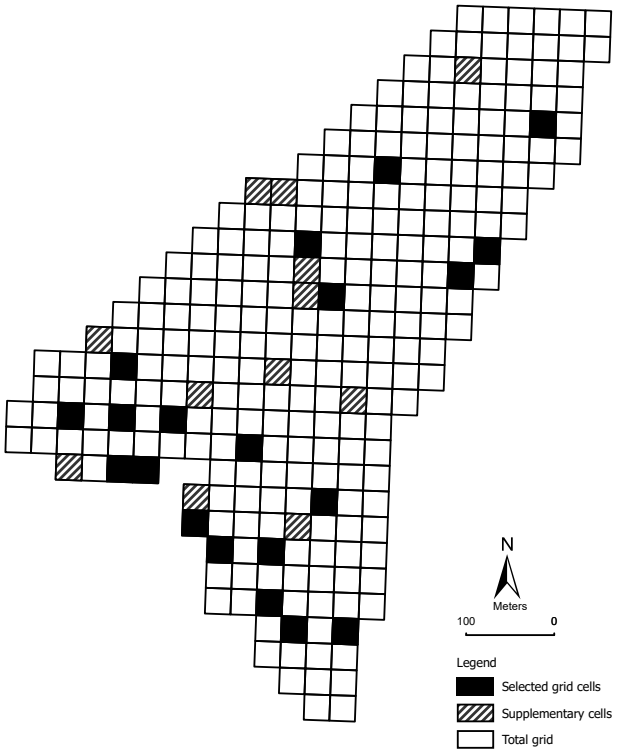

Figure 1: Schematic illustration of the 268 cells (20 m x 20 m) covering the entire grassland Alp Stabelchod. 20 grid cells containing at least one ant mound were randomly selected and used for soil and vegetation sampling. 12 additional cells were randomly selected for mound count validation.

Additionally, to the 20 selected cells, 12 more cells (Figure 1) were randomly selected for the validation of mound count data obtained via remote sensing (Chapter 2.6).

2.3 Soil sampling

Soil cores of 5 cm diameter and 10 cm depth were collected using a stainless-steel corer (AMS Samplers, American Falls, Idaho, USA) on June 9 (Figure 2). All samples were dried at 60°C in an oven (Binder, Tuttlingen, Germany), weighed and then sieved for 30 seconds at an amplitude of 0.5 mm with

a 2 mm sieve insert (Analysette 3 PRO, FRITSCH, Germany). Any ants found within the samples were carefully removed and large clumps of soil were crushed in a mortar prior to sieving. The sieved soil samples were ground for 3 minutes at a frequency of 300 s^{-1} using a mixing mill (MM400, Retsch®, Germany) and then analyzed for total C and N concentrations (Leco TruSpec Analyser, LECO Corporation, St. Joseph, Michigan, USA). The bulk densities of the material from the aboveground part of mounds and off the mounds were available from former years. For measuring the bulk density of the belowground part of mounds additional soil cores from 10 randomly selected mounds were taken, dried at 105°C for 24 hours and weighed.

2.4 Vegetation sampling

The aboveground vegetation samples were collected on June 19, when the vegetation development was advanced, but slightly prior to peak biomass. The vegetation in an area of 10 cm x 10 cm (1) on the south-facing edge of the mound and (2) at a distance of 2 m from the mound center, the south-facing part of the edge of the mound was clipped at ground level and placed in paper bags (Figure 2). The samples were dried at 60°C and ground for 2 minutes at a frequency of 300 s^{-1}. Total C and N concentrations were thereafter analyzed (Leco TruSpec Analyser, LECO Corporation, St. Joseph, Michigan, USA).

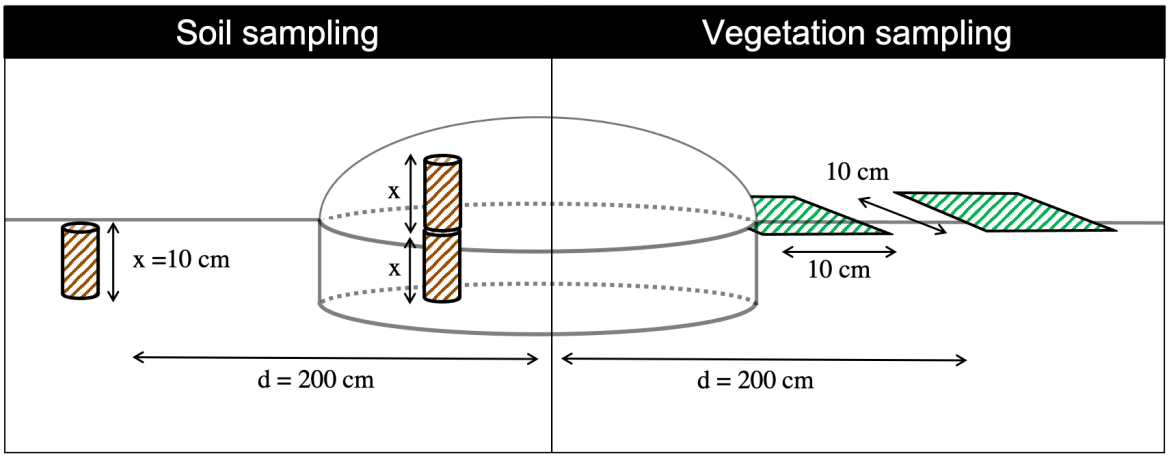

Figure 2: Schematic illustration of the sampling method. Soil cores of 10 cm height and 5 cm diameter were extracted on the mound, directly under the mound and at a distance of 2 meters from the mound center. The vegetation from an area of 10 cm x 10 cm was cut on the mound edge and at a distance of 2 meters from the mound center.

2.5 Counting ant mounds using remote sensing

The flight was performed with an ASCTEC Falcon 8 (Intel®, California, USA) octocopter equipped with a long wave infrared (LIR) thermal camera FLIR Tau® 2 640 (Teledyne FLIR LLC, Oregon, USA; spectral band 7.5 - 13.5 µm; Figure 3) on June 15, 2022. The ASCTEC Navigator software (Intel®, California, USA; *v.3.4.4*) was used for flight planning, installed on a laptop which acted as ground station to control the flight in real-time (Rossi et al., 2021). Due to battery life limitations, flight planning was optimized to minimize flight time. For this purpose, the flight was performed at an altitude of 60m with a forward and side overlap of approximately 50% and the outermost corner points were removed from the ideal flight plan. Three landings were needed for battery changes to cover the entire grassland area. The weather conditions were sunny with light winds and a mean temperature of 12.6° C (T_{min} = 0.3°C, T_{max} = 22.8°C). Temperature differences between mounds and the surrounding vegetation were found to be largest between noon and sunset (Appendix A.1), the flights were performed between 15:30 and 17:00 hrs. The south-western part of the pasture had to be re-imaged on July 7 at 12:00 because the thermal orthomosaic generated was distorted due to the high vertical structure of trees in the area. Data acquisition was performed at the same altitude with a forward and side overlap of 60%.

Geotags were assigned to the images using ASCTEC Navigator. Pix4D Mapper (Pix4D S.A., Prilly, Switzerland; *v.4.5.6*) was used for orthorectification using structure from motion (Westoby et al., 2012), to transform and combine the collected images into a thermal orthomosaic of the area. 26 Ground Control Points (GCP) were evenly distributed over the entire grassland and used for georeferencing: 8 of these GCP were noticeable structures, which were marked in the field using white plastic panels. Additionally, I selected the 18 largest of the 200 mounds, of which coordinates and the diameters were measured as GCP. Their coordinates were assigned to the images by identifying the largest mound in the images that matched the coordinate.

Further data processing was performed in ArcGIS Pro 2.7.0 (ESRI, California, USA): The thermal layer was rectified based on 141 control points using a spline transformation (Georeferencing toolbar). The ArcGIS Pro 2.7.0 Deep Learning toolset was used to label ant mounds for deep learning and to train Region Based Convolutional Neural Networks (R-CNN). To train the R-CNNs, two training areas were defined that covered a broad gradient with different tree, shrub and grass dominance. In these training areas, the thermal layer was manually searched and a total of 300 mounds were identified, labelled and

exported as training data for the R-CNN. 10% of the training data was assigned to be used as validation dataset during the model training. The following model settings were compared: two backbone models (Resnet50; Resnet100), batch sizes (2; 8), and confidence thresholds (50%; 75%) at which a mound was classified as such. To evaluate the model's accuracy, the F-score (Sasaki, 2007) was calculated in ArcGIS Pro 2.7.0.

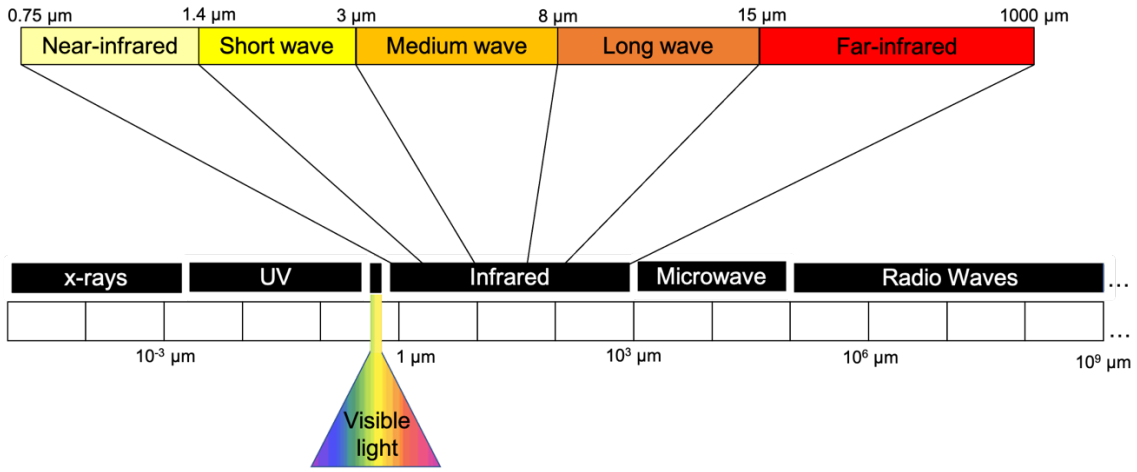

Figure 3: Schematic illustration of the classification of the electromagnetic spectrum into bands. The figure is adapted from PROTHERM (retrieved on January 15 from *https://www.pro-therm.com/infrared_basics.php*). The sensor used in this study is sensitive for the long wave region of infrared.

2.6 Training independent validation of mound counts

All ant mounds in the 20 selected grid cells used for soil and vegetation sampling and all mounds in the 12 additionally selected cells were counted *in situ*. This data was used to validate the Deep Learning model outputs. I used RStudio (RStudio Team, 2021; *v 1.4.1106*) to fit a linear regression for predicted (field survey) versus observed (detected by R-CNN) mounds and analyzed the Root Mean Squared Errors (RMSE) for the models. The model with the lowest RMSE was considered the best model.

2.7 Determination of mound diameter and height

I calculated the diameters of the mounds detected by the deep learning model in ArcGIS Pro 2.7.0 overlaying a *Minimal Bounding Rectangle* on each mound and deriving its perpendicular diameters D_1 and D_2 (Figure 4). A Generalized Additive Model (GAM) from the mgcv package (Wood, 2011*, v 1.8-38.1*) was used to predict the height based on the average diameter. The GAM was based on height

and diameter data of a total of 2309 mounds: 200 of which were the mounds measured in 2021 and the rest from field measurements obtained in 1998 and 2007.

2.8 Calculation of C and N pools

I first calculated the volume of each mound V_1 using the formula of half an ellipsoid (Risch et al., 2005; Sudd et al., 1977). The belowground mound volume V_2 was assumed to be elliptic-cylindrical, with depth x corresponding to the extracted soil sampling depth of 10 cm. For the volume of the surrounding reference soil matrix V_3, the area covered by mounds was subtracted from the total area of the respective grid cell and multiplied by 10 cm (Figure 4).

For all three sampling locations separately (above- and belowground mound parts, off mound), I multiplied the bulk density (BD_i) with the soil C or N concentration (NC_i) and the volume (V_i) to calculate the total N and total C pools [kg] (Figure 4). Total N and C pools were calculated for each mound and each grid cell individually, summed up for each sampling location and then divided by the total pasture area to calculate the contribution of each sampling location to the total N and C pools in the pasture. The contribution of vegetation to the pools has not been considered.

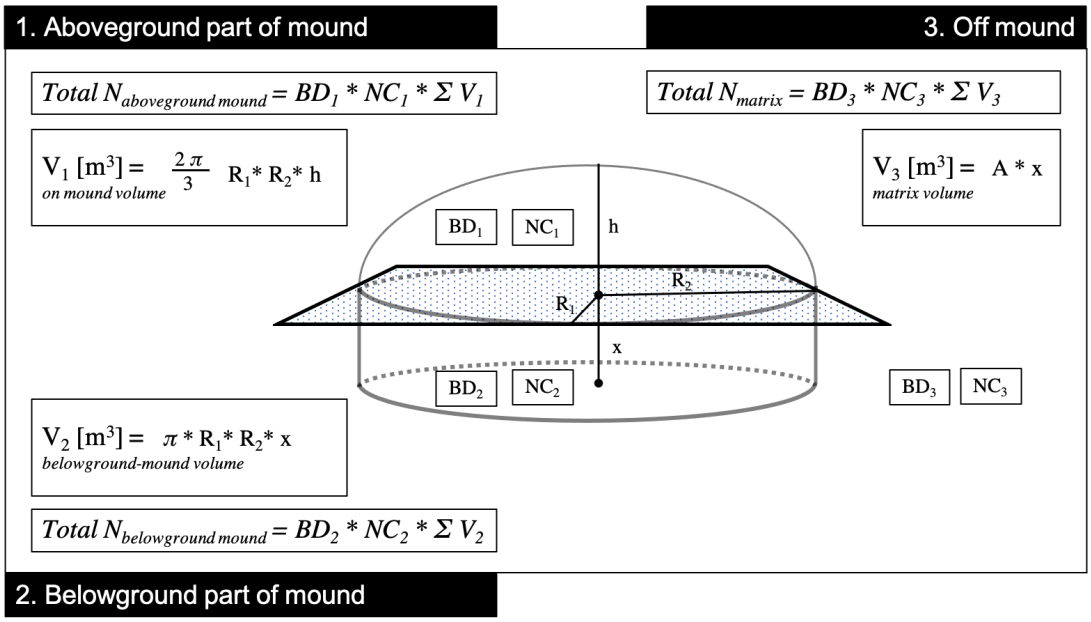

Figure 4: The formulas used for the calculation of volumes and total nutrient content of the different sampling locations *(aboveground and belowground mound, off mound)* are given. A schematic illustration visualizes how the different parameters were collected. The average bulk densities (BD_i) and nutrient concentrations (NC_i) were calculated for each sampling location. Radii R_1 and R_2 were calculated by overlaying a *Minimal Bounding Rectangle (dotted rectangle)* in ArcGIS Pro 2.7.0 and height h was derived from the average radius via fitting a GAM on diameter and height data available. The variable x corresponds to the sampling depth extracted with the stainless-steel corer.

2.9 Statistical analyses

Statistical analyses were performed in R (R Core Team, 2021; *v 4.0.5*) using RStudio (*v 1.4.1106*). Alpha was set to be 0.05. Graphics were created using the ggplot2 package (Wickham, 2016; *v 3.3.5*). To assess differences between the total soil N and C concentrations between the three sampling locations (*aboveground and belowground mound, off mound*), I fitted a linear mixed effects models with the lmer function in the lme4 package (Bates et al., 2015; *v 1.1-27.1*) and used the lmerTest package (Kuznetsova et al., 2017; *v 3.1-3*) to calculate p-values. In all models, sampling location was used as a fixed effect, the nest ID as a random effect. In case of significant differences, pairwise comparisons between the sampling locations were tested using a post-hoc test from the emmeans package (Lenth, 2021; *v 1.7.0*). To compare the bulk densities of the three sampling locations, I used a one-way ANOVA.

To analyze the mound distribution patterns over time, density maps, the differences per grid cell, and an Optimized Hot-Spot Analysis (Spatial Statistics Toolset) were calculated in ArcGIS Pro 2.7.0.

.

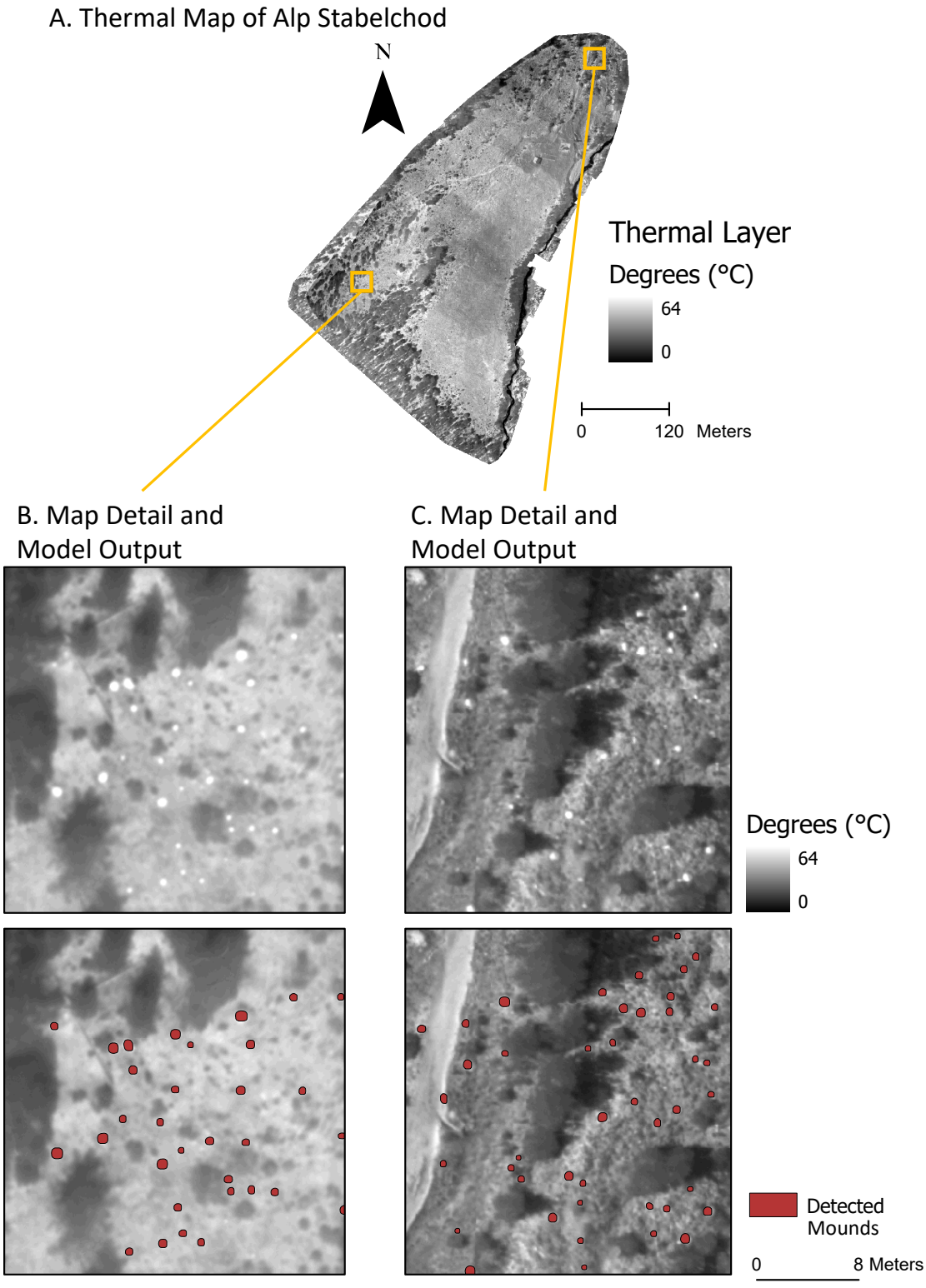

Figure 5: The orthorectified and georeferenced thermal layer of Alp Stabelchod serves as an overview (A). More detailed extracts are given in B and C with the corresponding model outputs where the detected mounds are marked in red. In the thermal image *F. exsecta* mounds appear as spots of high temperature (white), surrounded by cooler vegetation (grey).

3 Results

3.1 Remote Sensing

3.1.1 Image Processing and visual inspection

The quality report from the initial processing of the images showed a suboptimal extractable visual content and therefore only 92% of the images were used for the calibration of the orthomosaic. However, the results were reported to be likely of high quality in the calibrated areas (Appendix A.2). A major error was reported for georeferencing. 26 Ground Control Points (GCP) were used for georeferencing resulting in an overall mean GCP error of 0.12 m in x-direction and 0.07 m in y-direction.

Upon an initial visual inspection of the images, the mounds appear to be well distinguishable as round white spots (high temperature) from the surrounding vegetation (Figure 5). In particular, temperature differences between the mounds and the surroundings often differed by more than 10° C, with mound surfaces regularly reaching temperatures between 40°C and 55°C based on the thermal image (Figure 5; see also Appendix A.1).

3.1.2 Detecting *Formica exsecta* mounds using deep learning

Comparing the deep learning model metrics, Resnet50 was found to be the more suitable backbone model than Resnet101 (data not shown) and the average precision score (aps) after 20 epochs was higher using a batch size of 2 (aps = 0.71), compared to a batch size of 8 (aps = 0.65). The Region Based Convolutional Neural Networks (R-CNN) model based on the thermal layer reached an accuracy of F-Score = 0.79 in detecting the mounds. The model output validation using the independent field survey data showed that the RSME were smallest, when the confidence threshold at which a mound was classified was set to 50% (Figure 6), resulting in a RSME = 5.84.

An object detection model (Mask R-CNN based on Resnet50 and batch size 2) applied to the thermal layer was therefore found to be the best suited model, as the RMSE was lowest. Overall, the model appeared to underestimate the number of mounds compared to the mound numbers obtained by the field survey (Figure 6).

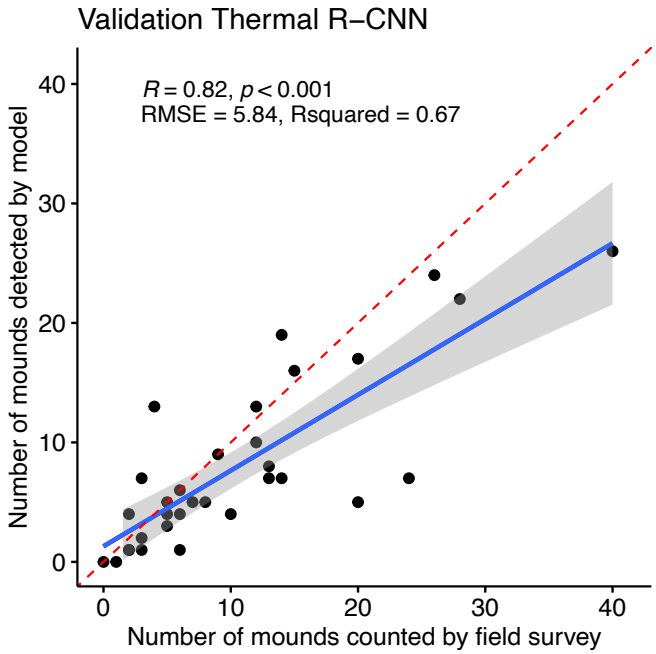

Figure 6: Linear regression (blue) between the number of *F. exsecta* mounds observed by field survey (x-axis) and the number of mounds predicted by the Deep Learning model (y-axis) at a classification threshold of 50%. The red dashed line corresponds to a 1:1 ratio. RMSE, R-squared and p-values are given in the plot.

3.2 Temporal ant mound patterns

A total of 783 *F. exsecta* mounds were counted in the field survey of 1998, giving an average density of 73.17 mounds ha^{-1} with a maximum density of 500 mounds ha^{-1}. The average mound diameter in 1998 was 36.0 cm, the maximum 146 cm. In 2007, there were 1333 mounds, which corresponds to almost a doubling in counts between these two time points. The average density was 124.58 mounds ha^{-1}, the maximum 1000 mounds ha^{-1}. The average mound diameter increased to 42.8 cm, the maximum diameter detected was 160.0 cm. In 2021, I detected a total of 1655 mounds with remote sensing. The average density was 154.7 mound ha^{-1} with a maximum of 775 mounds ha^{-1}. Even though I likely underestimated the total number of mounds using the deep learning model (Figure 6) there was still an increase in the number of mounds between 2007 and 2021, but this increase was smaller than between the first two time-steps. The mean diameter of the ant mounds measured in 2021 was 56.0 cm, with a maximum of 109.3 cm.

Regardless of when ant mounds were counted, there was an area with low mound counts in the central eastern part of the pasture, which borders to the river, and areas with a higher density of mounds close to the northern, southern and south-western forest edge (Figure 7). These findings were supported by the results of an Optimized Hot-Spot-Analysis which can be found in Appendix A.3. It shows a stable cold spot in the central-eastern part as well as the three hot spots close to the forest edge. The areas with higher mound densities near the edge of the forest showed a particularly strong increase in the number of mounds between 1998 and 2007, but showed a reduction in numbers between 2007 and 2021 (Figure 8).

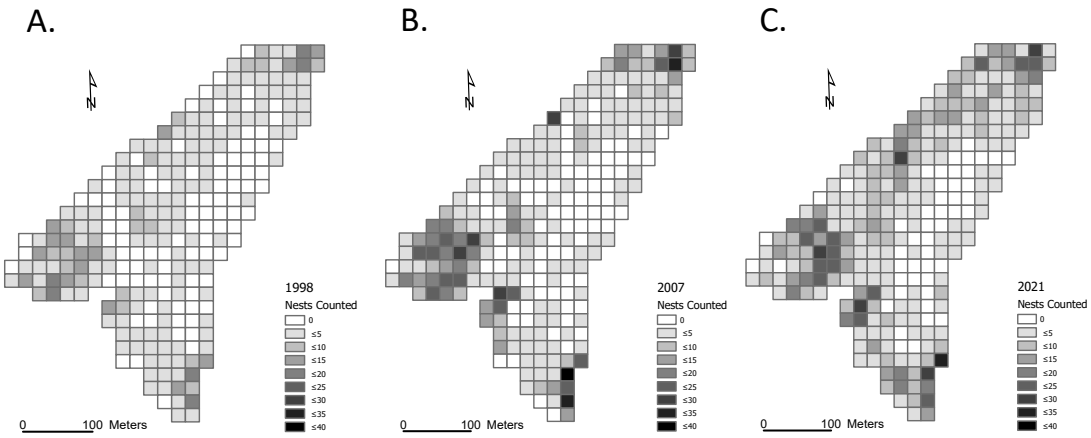

Figure 7: Grid-wise count data of *F. exsecta* mounds from the years A. 1998, B. 2007 and C. 2021. In white colored fields, no mounds were detected, darker colors indicate higher counts.

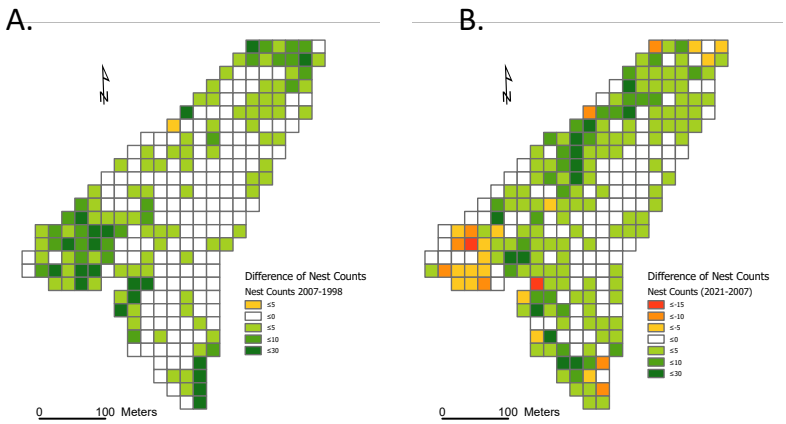

Figure 8: Grid-wise count differences of *F. exsecta* mounds between the timepoints (A.) 2007 – 1998 and (B.) 2021 – 2007. White cells indicate no change. Orange to red cells indicate a mound reduction, fair green to dark green an increase between the two respective time points.

3.3 Soil and vegetation properties

3.3.1 Soil C and N concentrations

Figures 9 and 10 visualize the relationship of total soil nitrogen (N) and carbon (C) concentrations between the three sampling locations (aboveground, belowground, off ant mound) across the 20 mounds sampled. No significant difference was found in total soil N concentration between the aboveground and belowground mound material ($p = 0.88$; Figure 9 A). In contrast, total soil N concentration of both aboveground ($\beta = 0.38$, $SE = 0.08$, $t_{60} = 4.62$, $p < 0.001$; Figure 9 B) and belowground mound material ($\beta = 0.34$, $SE = 0.08$, $t_{60} = 4.10$, $p < 0.001$; Figure 9 C) significantly differed from off the mound soils. The aboveground mound material contained a slightly higher total soil C concentration than the belowground mound material ($\beta = 2.58$, $SE = 1.04$, $t_{60} = 2.47$, $p = 0.04$; Figure 10 A). Both the aboveground ($\beta = 8.82$, $SE = 1.03$, $t_{60} = 8.55$, $p < 0.001$) and belowground mound material ($\beta = 6.24$, $SE = 1.04$, $t_{60} = 5.99$, $p < 0.001$, Bonferroni corrected) contained significantly higher total soil C concentrations than the off the mound soil (Figure 10 B and 10 C). Surprisingly, there were no differences found in soil C/N ratio between the three sampling locations.

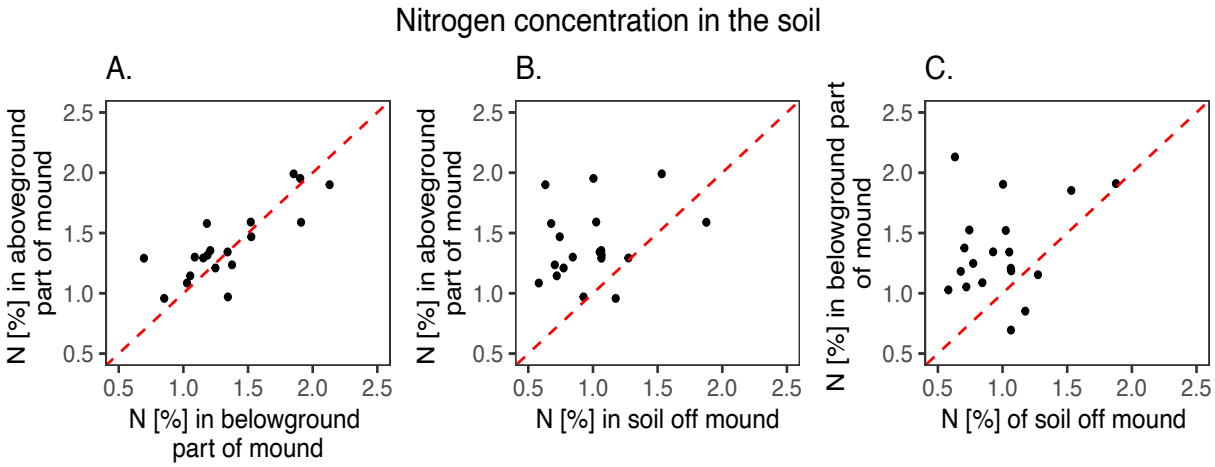

Figure 9: Relationships between soil N concentration [%] from (A) aboveground (y-axis) versus belowground (x-axis) parts of ant mounds, (B) aboveground parts of mounds (y-axis) versus off the mounds soil (x-axis) and (C) belowground parts of ant mounds (y-axis) versus off the mounds soil (x-axis). The red dashed line corresponds to the 1:1 ratio.

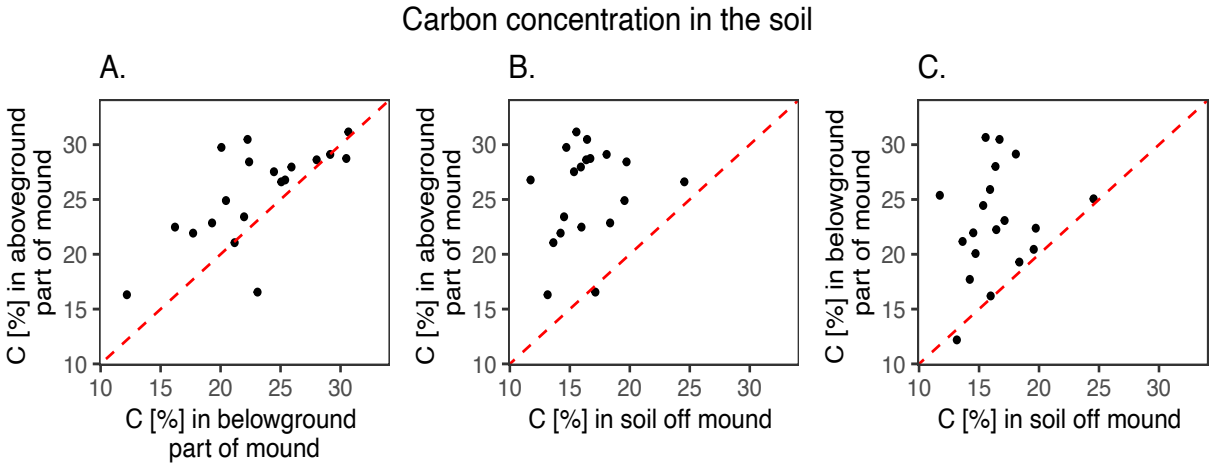

Figure 10: Relationships between soil C concentration [%] from (A) aboveground (y-axis) versus belowground (x-axis) parts of ant mounds, (B) aboveground parts of mounds (y-axis) versus off the mounds soil (x-axis) and (C) belowground parts of ant mounds (y-axis) versus off the mounds soil (x-axis). The red dashed line corresponds to the 1:1 ratio.

3.3.2 **Soil bulk density**

The aboveground mound material had a significantly lower bulk density than both the belowground mound material (β = -277, SE = 54.9, t_{33} = - 5.05, p < 0.001) and the off-mound soil (β = -422, SE = 51.6, t_{33} = - 8.173, p < 0.001). The difference in bulk density between above- and belowground mound material was less pronounced, but still significant, with the belowground mound material having a lower bulk density (β = -144, SE = 51.6, t_{33} = - 2.80, p = 0.02).

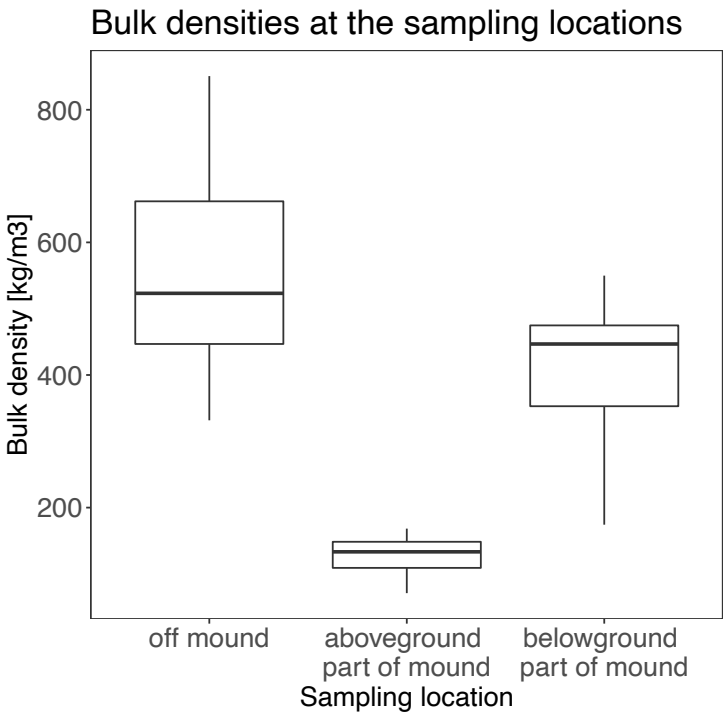

Figure 11: Soil bulk density [kg m^{-3}] is plotted for the three sampling locations: The surrounding reference soil, the soil sampled from belowground part of the ant mounds and the soil sampled from the aboveground part.

3.3.3 Vegetation C and N concentrations

Similarly to the soil samples, the N concentration in the vegetation growing on ant mounds was higher than in the one growing off the mounds (β = 0.21, SE = 0.07, t_{40} = 2.88, p = 0.01; Figure 12 A). More pronounced, but the other way around, was the difference in vegetation C concentration between the two sampling locations: The vegetation sampled off the ant mounds contained significantly more C than the vegetation growing on the mounds (β = 0.59, SE = 0.12, t_{40} = 5.10, p = 0.01; Figure 12 B). In contrast to the soil C/N ratio, the C/N ratio in the vegetation growing on the ant mounds (mean = 20.08, SD = 4.53) was significantly lower than that in the vegetation growing off the mounds (mean = 22.42, SD = 5.08; β = -2.34, SE = 0.86, t_{40} = -2.72, p = 0.01).

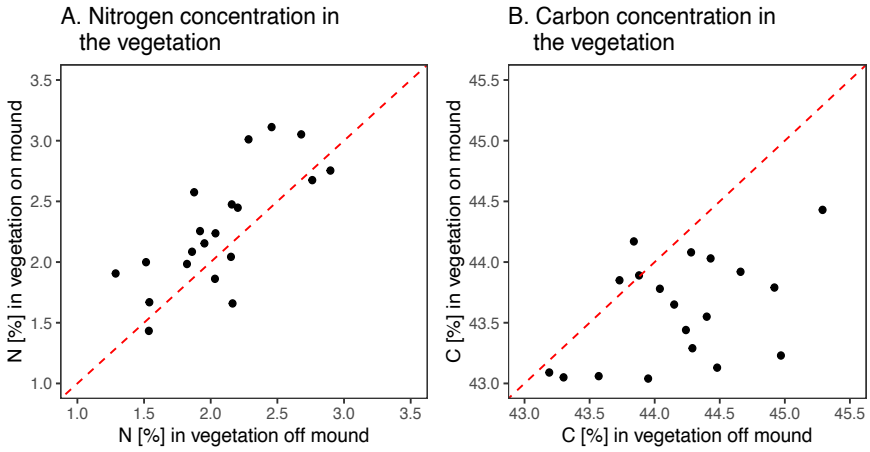

Figure 12: Relationships between vegetation sampled on ant mounds (y-axis) versus off mounds (x-axis) regarding (A) nitrogen concentration [%] and (B) carbon concentration [%]. The red dashed line corresponds to the 1:1 ratio.

3.4 C an N pools

3.4.1 Mound heights and diameters

I fitted a univariate GAM to explore the relationship between the average diameter and height of an ant mound: Height ~ s(Average Diameter) (n = 2309). The model was highly significant (p < 0.001) and approximately cubic (estimated degrees of freedom = 3.34). Only 23.3% of the deviance was explained by the average diameter (adj. Rsquared = 0.233). Height increased with average diameter, showing a saturation at around height of 17 cm at a diameter of around 60 cm (Figure 13). I used this GAM model to predict the height for the mounds detected by the deep learning model, despite the rather low deviance explained, as the diameter was the only parameter available in this case.

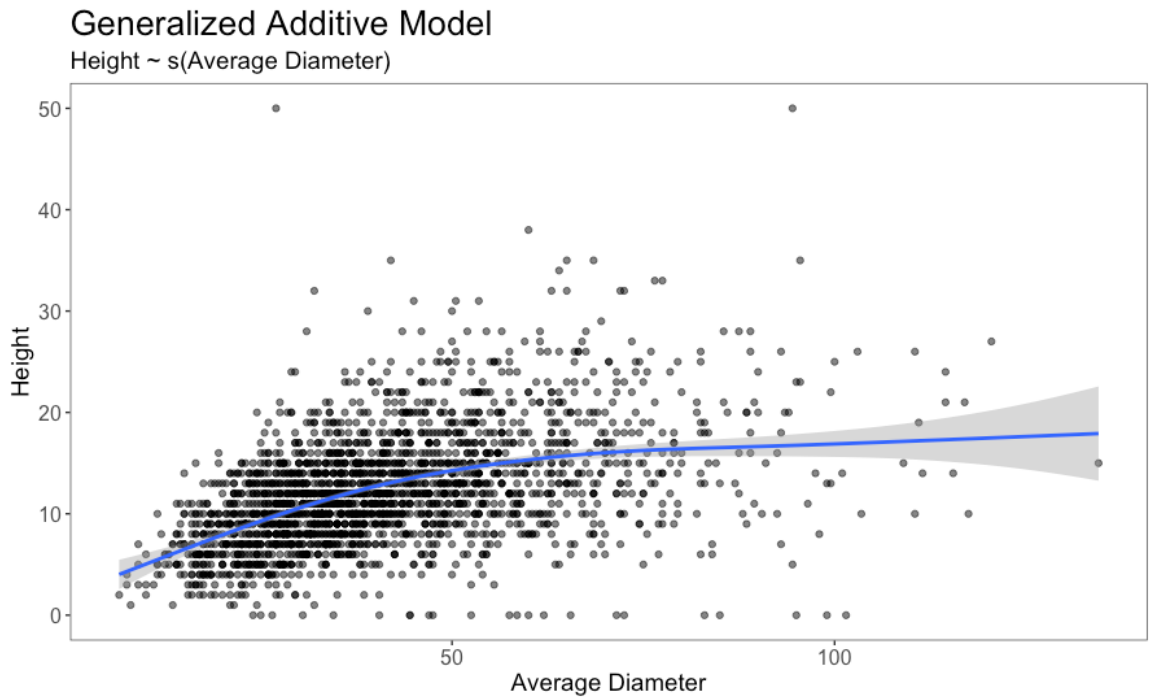

Figure 13: Univariate GAM fitted to explore the relationship between the average diameter (x-axis) and height of an ant mound (y-axis): Height ~ s(Average Diameter), (n = 2309). The model was highly significant for the smooth term ($p < 0.001$) and approximately cubic (estimated degrees of freedom = 3.34).

3.4.2 Contribution of ant mounds to the overall C and N pool

The contribution of the aboveground and belowground parts of the mounds to the overall C and N pools measured for the 10 cm soil depth on Alp Stabelchod was 0.55% for soil C pools and 0.53% for soil N pools (Table 1). The belowground part of the mound contributes more to the overall pools of the grassland than the aboveground part of the mound, but the overall contribution is small. The area contribution of the mounds to the entire grassland area is small (0.4%; Table 1).

Table 1: Total soil C and total soil N pools for the three sampling locations in relation to the grassland area they cover.

	Total C			Total N			Area	
	Pool [kg ha^{-1}]	Contribution [%]		Pool [kg ha^{-1}]	Contribution [%]		Total [ha]	Contribution [%]
Aboveground part of mound	1'197.1	0.14	0.55	65.7	0.13	0.53	0.045	0.4
Belowground part of mound	3'424.0	0.41		18.8	0.40			
Surrounding reference soil	837'032.8	99.45		50311.8	99.47		10.63	99.6

4 Discussion

4.1 Detection of ant mounds using remote sensing

Most previous studies focused on the application of airborne or satellite near infrared (NIR) imagery with sensors covering wavelengths from 400 nm to 1000 nm to detect ant nests (Fletcher et al., 2007; Green et al., 1977; Vogt, 2004b; Vogt & Wallet, 2008). Although they successfully detected mounds, shortwave NIR imagery was shown to have limitations (Vogt & Oliver, 2006) and may not fully meet the requirements for application (Song et al., 2020), as the differences in reflectance between ant nests of red fire ants (*S. invicta*) and standard soil were not significant in the visible and short wavelength regions of NIR.

In this study I used a thermal - long infrared (LIR) - sensor that covers considerably longer wavelengths than these critical NIR regions. The results of my study clearly showed that counting *F. exsecta* mounds in grasslands with a LIR camera mounted on an UAV is meaningful. The mounds appear as characteristic white elliptic dots of high temperature surrounded by cooler vegetation. These findings are supported by those of Vogt et al. (2008), who considered the temperature differences between *S. invicta* mounds and their surroundings sufficient for detection using thermal infrared remote sensing. The temperature difference between *F.exsecta* mounds and their surroundings were even larger than those reported for *S. invicta* (Vogt et al., 2008). Also, Wylie et al. (2021) used mid infrared and LIR sensors to detect *S. invicta* in Australia, which proved to be highly successful.

Despite the successful detection of *F. exsecta* ant mounds on Alp Stabelchod, the total number of mounds is probably underestimated. There are several improvements to the method that could further improve the detectability of mounds. Due to the drone's limited battery life, I was only able to fly with a low overlap, which resulted in suboptimal extractable image content. In addition, the low overlap in combination with the complex data patterns of shaded versus sunny areas due to single trees or shrubs or the vicinity of the forest edge led to a low number of matches in some images.

The main flight to obtain the thermal images was conducted between 15:30 and 17:00 as I sought to maximize the differences in surface temperatures between mounds and the surrounding vegetation. This approach had the drawback of producing more shadow effect by trees, than when flying closer to

solar noon as I did with the additional flight that was necessary. Both the temperature logger data and the data gathered with this additional flight showed, that the temperature differences around solar noon are already sufficient to distinguish *F. exsecta* mounds from the surroundings, while the shadows can be significantly reduced. I would therefore suggest to conduct future flights around solar noon. This goes along with the findings of Vogt et al. (2008), who also hypothesized that when the overall difference between mean mound temperature and its surrounding is critical, data acquisition might be best undertaken around solar noon.

Another potential improvement for mound detection could potentially be made if all mounds in specific grid cells would be georeferenced. This would prevent the labelling of false-positive or false-negative data during the training of the deep learning model, and also allow an analysis of which characteristics of mounds were associated with a poor detection success. Considering, for example, the diameter distribution of the detected mounds (Appendix A.4) it seems likely that, in particular, small mounds were not detected. The diameter of the smallest detected mound was close to the mean diameter in previous years. The effectiveness regarding detection of relatively small targets was reported to be dependent upon spatial resolution of the data (Vogt et al., 2008). A lower flying UAV would probably solve this issue. Hence, summarized, a UAV with a longer battery life, that would allow for a longer flight time where a lower flight line with higher overlap could be flown, would likely result in much higher detectability of ant mounds.

4.2 Temporal and spatial patterns in the occurrence of *F. exsecta* mounds

F. exsecta has increased strongly on Alp Stabelchod since the year 1998, especially between 1998 and 2007 with almost a doubling of mound numbers. But also between 2007 and 2021 the supercolony sustained well and has continued to grow to a total number of 1655 mounds. This is surprising insofar as *F. exsecta* populations declined significantly in Central Europe since 1950 (Seifert, 2000). However, this decline was mainly driven by a change of management in forestry and agriculture, for example by afforestation of clearings and meadows, intensified cattle pasturing or intensive use of mineral fertilizers and liquid manure (Seifert, 2000). Under the no-management strategy of the SNP, the environmental conditions on Alp Stabelchod remained largely unaltered and allowed the supercolony to grow to a

remarkable size. Even though it seems relatively small compared to the largest reported *F.exsecta* supercolony of 3347 mounds in Transylvania, Romania (Markó et al., 2012), Alp Stabelchod's colony has outgrown the one reported as the second largest colony in Europe (Wiezik et al., 2017), which is located in the Carpathian Mountains in Slovakia (1487 mounds). However, the mean mound density of Stabelchod's supercolony lays within the range of findings from other studies. Although the 154.7 mounds ha^{-1} I counted on Alp Stabelchod on average is well below the mean mound density of 316.7 nests ha^{-1} described in the Slovakian supercolony by Wiezik et al. (2017), it corresponds closely to the density (153.2 mounds ha^{-1}) observed by Markó et al., (2012) in Romania and which was also reported to be a medium density for supercolonies at a large spatial extent (e.g. Kümmerli & Keller, 2007 *as summarized in* Markó et al., 2012).

The mounds of *F. exsecta* were not distributed homogenously over the grassland Alp Stabelchod. They were clustered in "hot spots" of high densities, with a large area with low mound counts in the central eastern part of the pasture, south of the hut. Interestingly, the area of low mound densities corresponds to the part of the grassland that was reported as phosphorous enriched due to irrigation back in times of agricultural use (Schütz et al. 2003). These authors identified this part of the pasture as area with the highest grazing pressure by red deer. The question therefore arises, whether the distribution of *F. exsecta* mounds could be at least partly influenced by red deer. It was previously hypothesized, for example, that disturbance caused by red deer, such as trampling or the removal of nesting or foraging material, displaces *F. exsecta* into the less heavily grazed areas (Schütz et al., 2008). However, despite the fact that intensive grazing is assumed to reduce population density of *F. exsecta* (Seifert, 2018), the meadow with the large supercolony in Romania is fairly intensely grazed by cows for most of the year (Markó et al., 2012). Similarly, also the Slovakian site was cattle grazed (Wiezik et al., 2017). The «painful biting» (Seifert, 2018) and generally aggressive behavior of *F. exsecta* against intruders (Erős et al., 2009; Wiezik et al., 2017) thus seems to allow at least partly defense against disturbances through grazing. Another possible explanation for the high densities of mounds on these cattle pastures could also be that cattle generally follow a diurnal rhythm with most grazing during daylight and little grazing at night (Kilgour, 2012; Sambraus et al., 1978). Red deer, in contrast, spend a much higher proportion of their grazing during the night (Hester et al., 1996). This is particularly true for the SNP where red deer avoid the pastures during daytime when visitors are present and graze at night (Leuzinger, 1999 *cited in* Schütz et al., 2003). Like most species of the genus *Formica* (Seifert, 2018), I observed *F. exsecta* to

forage diurnally. During the night, when the ants are less active, they might not be able to defend themselves and their mounds effectively and therefore avoid the part of the pasture exposed to heavy grazing by red deer.

Another possible explanation for the very heterogenous distribution of *F. exsecta* mounds on Alp Stabelchod could be related to the distance to the forest edge. The importance of forest edges has already been emphasized by Maggini et al. (2002) who found a majority of *F. exsecta* colonies within the SNP in forest edge ecoclines. Despite its wide range of possible food sources, aphid tending covers a major portion of the energy needs of *F. exsecta*, with *Lachnidae* (tree aphids) being the main trophobionts in coniferous and deciduous forests (Seifert, 2018). At least permanent auxiliary mounds of *F.exsecta* have been reported to be most commonly built near constant sources of aphid colonies like trees, shrubs and perennial herbs (Goryunov, 2015). Erős et al. (2009) found high densities of *F.exsecta* mounds close to aphid colonies, and also Kilpeläinen et al. (2005) suggested that aphids should deserve more emphasis in the distribution studies of aphid-tending ants.

It remains to be seen how the supercolony on Alp Stabelchod will develop in the future. The density maps presented in this study show partial decreases in the number of mounds, mainly close to the forest edge, where particularly high densities have been counted in the past. In the Alps, in a majority of abandoned areas, natural forest re-growth is observed (Tasser et al., 2006). A spatio-temporal secondary succession model predicted that *Pinus mugo* will invade Alp Stabelchod from the edges to the center within 200 years after the foundation of the SNP (Wildi, 2002). So far, this prediction can most likely not be verified, as most of the pasture still remains open after over 100 years of protection since 1914. However, it is likely that the growth of the trees present and slowly advancing forest edges will lead to adverse conditions for *F. exsecta*, which depend on direct sunlight to maintain stable temperatures inside their mounds (Seifert, 2000). Hence, it is possible that in the longer term a shift of the regions of high densities from the hot-spot areas towards the center of the meadow might be observed. Dobrzanska (1973) found evidence that migration is a constant element in the behavior of *F. exsecta* and displacements of *F. exsecta* mounds have already been described by Goryunov, (2015): “At some time, an anthill may become constantly overshadowed by growing vegetation. In such cases, the primary *F. exsecta* nest may travel a distance of about 1.5 m in several weeks with only the intermediate layer and subterranean part left at the former site. Gradual relocations of primary anthills

may last for years with several centimeters traveled each year." However, it cannot be ruled out that the observed decrease in this area may in fact be due to ant mounds at the bases of trees or in tree shade being particularly difficult to detect using remote sensing (Wylie et al. 2021).

4.3 C and N accumulation in *F. exsecta* mounds

Overall, I found significantly higher total soil N and soil C concentrations in the mounds of *Formica exsecta* compared to the surrounding soil off the ant mounds. The high levels of C and N in ant mounds are generally attributed to the accumulation and consumption of high amounts of prey, honeydew and organic waste (Bierbaß et al., 2015; Cammeraat & Risch, 2008; Frouz et al., 2003). There have also been experiments on whether this accumulation could be related to altered nutrient cycling rates via cascading effects through top-down regulation of decomposers or other predator species by ants (Cates et al., 2021). Such an effect on nutrient cycling rates via cascading effects has indeed been found for predators, such as spiders (Schmitz, 2009; Strickland et al., 2013), but not for ants (Cates et al., 2021). However, an effect of ants on the abundance of decomposer or predator abundances and thus on the ratios between different trophic organism groups has been shown (e.g. De Almeida et al., 2020; Wills & Landis, 2018), which might be an indication that nutrient cycling might be influenced as well.

To the best of my knowledge, the influence of *F. exsecta* on the concentration of N and C in soils has not been quantified to this date, but has been assessed for other ant species. Wang et al. (2017) reported, for example, that three underground-nesting ant species in a tropical forest in China had higher total organic C and higher total N concentrations in their nests compared to the surrounding soil. Elevated N and other soil nutrients concentrations relative to the surrounding were also reported for the ant *Pogonomyrmex rugosus* in arid areas of North America (Snyder et al., 2002; Wagner & Jones, 2006). In grasslands, some studies reported higher concentrations of soil N in nests of *Lasius flavus* compared to the surrounding soil (Platner, 2006 p. 121; Wu et al., 2010), while others found lower concentrations of C and N inside *Lasius sp*. nests (Dean et al., 1997; Dostál et al., 2005). It was suggested that the effect varies with ant species (Wang et al., 2017). However, a recent meta-analysis by Farji-Brener & Werenkraut (2017) provided quantitative evidence that suggests that the effect is quite general across several ant groups and habitats.

The lower bulk densities I found in the ant mounds compared to the soil off mounds align well with the existing literature. The excavation of soil material during ant nest construction which includes the production of galleries and chambers is generally known to increase the porosity of the soil, leading to lower bulk densities in the nests of various ant species (Baxter & Hole, 1967 *cited in* Folgarait, 1998; Lal, 1988 *and* Lobry de Bruyn & Conacher, 1990 *cited in* Cammeraat & Risch, 2008; MacMahon et al., 2000; Wang et al., 2017).

Overall, I was able to show that *F. exsecta* alters various soil properties locally with its mound building activities on Alp Stabelchod, which also has an impact on the vegetation. The higher N and lower C concentrations in the vegetation growing on the ant mounds compared to that growing off the mounds may directly be caused by the higher N concentration of mound material compared to the soils off the mounds since plants depend on the N available in the soil (e.g. Di Palo & Fornara, 2015). However, the differences in plant N and C concentrations may also be influenced by altered plant species composition, as the soil properties may be selectively favoring or disfavoring particular plant species (Alejandro Gustavo Farji-Brener, 2005; Garrettson et al., 1998; Silva et al., 2012 *cited in* Farji-Brener & Werenkraut, 2017). On Alp Stabelchod, Schütz et al. (2008) found significant and continuous changes in vegetation composition on gradients from *F. exsecta* mounds into the adjacent grassland, with mainly graminoids as dominant species on ant mounds and herbaceous plants and legumes with increasing distance from the mounds.

4.4 Grassland C and N pools

F. exsecta contributed to less than 1% to the soil C and N pools on Alp Stabelchod. Although this seems low, the values fall within range of the contribution of *Formica rufa* species to C and N concentrations in European forests (Kilpeläinen et al., 2007; Risch et al., 2005) or of *Lasius flavus, Lasius niger* and *Formica candida* to grassland pools in China (Wu et al., 2013). However, *F. exsecta* considerably increased the heterogeneity of C and N across the grassland: lower soil bulk densities were paralleled by higher total soil N and C concentrations. This appears to affect plant species composition (Schütz et al., 2008) and enhances vegetation nutrient concentrations and could thus possibly also influence other trophic levels, for example decomposers (Wills & Landis, 2018) or large primary consumers such as red deer that frequently and numerously visit the grassland to forage (Leuzinger, 1999). Particularly lactating

red deer hinds depend on nutritious forage (Clutton-Brock et al., 1987) and might benefit from mound building *F. exsecta*. In addition, the heterogeneity of soil C and N concentrations and pools is most likely not only enhanced at the local scale (within a two-meter radius of the nest), but also at larger scales, i.e., the entire grassland, when we consider the heterogeneous distribution of mounds across the grassland.

5 Conclusions

F. exsecta mounds were detectable using a UAV equipped with a longwave infrared thermal camera. However, it is important to optimize flight time and georeferencing to maximize the method output. It will depend on the research question, whether a remote sensing approach or a field survey approach is more suitable for future mound census. While the remote sensing approach may be well suited for the observation of individual mound dynamics at high temporal and spatial resolution, small mounds and mounds located in tall grass or at the base of trees may not be detected. To ensure that mound counts are not underestimated with remote sensing techniques, a UAV with a long battery life that allows for a low flight line and high overlap should be used. Otherwise, a field survey may still be the more reliable approach. It would also be conceivable to use a combination of both methods: Count mounds across the entire pasture with remote sensing and check the areas of higher uncertainty using field surveys.

The distribution of the mounds across Alp Stabelchod is likely a result of a trade-off between the proximity to food sources, a given minimum sunlight demand and a reduction of grazing pressure by red deer and the total number of mounds increased considerably between 1998 and 2007 and a bit less between 2007 and 2021. Yet, the contribution of *F. execta* mounds to the total N and C pools of the pasture was neglectable. However, this ant species can still be considered an important ecosystem engineer on Alp Stabelchod as it increases heterogeneity by locally altering soil properties and vegetation composition. In addition, the uneven distribution of nests increases heterogeneity at a larger landscape scale.

Bibliography

Achermann, G. (2000). *The influence of red deer (Census elaphus L.) upon a subalpine grassland ecosystem in the Swiss National Park.* ETH Zurich.

Bates, D., Mächler, M., Bolker, B., & Walker, S. (2015). Fitting Linear Mixed-Effects Models Using {lme4}. *Journal of Statistical Software*, *67*(1), 1–48. https://doi.org/10.18637/jss.v067.i01

Baxter, F. P., & Hole, F. D. (1967). Ant (Formica cinerea) Pedoturbation in a Prairie Soil. *Soil Science Society of America Journal*, *31*(3), 425–428. https://doi.org/10.2136/sssaj1967.03615995003100030036x

Bierbaß, P., Gutknecht, J. L. M., & Michalzik, B. (2015). Nest-mounds of the yellow meadow ant (Lasius flavus) at the “Alter Gleisberg”, Central Germany: Hot or cold spots in nutrient cycling? *Soil Biology and Biochemistry*, *80*, 209–217. https://doi.org/10.1016/j.soilbio.2014.09.020

Bundesamt für Umwelt Wald und Landschaft. (1994). *Rote Liste der gefährdeten Tierarten Schweiz*.

Cammeraat, E. L. H., & Risch, A. C. (2008). The impact of ants on mineral soil properties and processes at different spatial scales. *Journal of Applied Entomology*, *132*(4), 285–294. https://doi.org/10.1111/j.1439-0418.2008.01281.x

Cates, A. M., Wills, B. D., Kim, T. N., Landis, D. A., Gratton, C., Read, H. W., & Jackson, R. D. (2021). No evidence of top-down effects by ants on litter decomposition in a temperate grassland. *Ecosphere*, *12*(7). https://doi.org/10.1002/ecs2.3638

Clutton-Brock, T. H., Iason, G. R., & Guiness, F. . (1987). Sexual segregation and density-related changes in habittat use in male and female red deer (Cervus elaphus). *Journal of Zoology*, *211*(2), 275–289.

De Almeida, T., Blight, O., Mesléard, F., Bulot, A., Provost, E., & Dutoit, T. (2020). Harvester ants as ecological engineers for Mediterranean grassland restoration: Impacts on soil and vegetation. *Biological Conservation*, *245*(November 2019), 108547. https://doi.org/10.1016/j.biocon.2020.108547

Dean, W. R. J., Milton, S. J., & Klotz, S. (1997). The role of ant nest-mounds in maintaining small-scale patchiness in dry grasslands in Central Germany. *Biodiversity and Conservation*, *6*(9), 1293–1307. https://doi.org/10.1023/A:1018313025896

Del Toro, I., Ribbons, R. R., & Pelini, S. L. (2012). The little things that run the world revisited: A review of ant-mediated ecosystem services and disservices (Hymenoptera: Formicidae). *Myrmecological News*, *17*, 133–146.

Di Palo, F., & Fornara, D. (2015). Soil fertility and the carbon:Nutrient stoichiometry of herbaceous plant species. *Ecosphere*, *6*(12). https://doi.org/10.1890/ES15-00451.1

Dibner, R. R., Doak, D. F., & Lombardi, E. M. (2015). An ecological engineer maintains consistent spatial patterning, with implications for community-wide effects. *Ecosphere*, *6*(9), 1–17. https://doi.org/10.1890/ES14-00415.1

Dobrzanska, J. (1973). Ethological studies on polycalic colonies of the ants Formica exsecta Nyl. *Acta Neurobiologiae Experimentalis*, *33*(3), 597–622.

Dostál, P., Březnová, M., Kozlíčková, V., Herben, T., & Kovář, P. (2005). Ant-induced soil modification and its effect on plant below-ground biomass. *Pedobiologia*, *49*(2), 127–137. https://doi.org/10.1016/j.pedobi.2004.09.004

Drager, K. I., Hirmas, D. R., & Hasiotis, S. T. (2016). Effects of Ant (Formica subsericea) Nests on Physical and Hydrological Properties of a Fine-Textured Soil . *Soil Science Society of America Journal*, *80*(2), 364–375. https://doi.org/10.2136/sssaj2015.08.0300

Erős, K., Markó, B., Gál, C., Czekes, Z., & Csata, E. (2009). Sharing versus monopolizing: distribution of aphid sources among nests within a Formica exsecta Nylander (Hymenoptera: Formicidae) supercolony. *Israel Journal Entomology*, *39*, 105–127.

Escobar-Ramírez, S., Duque, S., Henao, N., Hurtado-Giraldo, A., & Armbrecht, I. (2012). Removal of nonmyrmecochorous seeds by ants: Role of ants in cattle grasslands. *Psyche (London)*, *2012*. https://doi.org/10.1155/2012/951029

Farji-Brener, Alejandro G., & Werenkraut, V. (2017). The effects of ant nests on soil fertility and plant performance: a meta-analysis. *Journal of Animal Ecology*, *86*(4), 866–877. https://doi.org/10.1111/1365-2656.12672

Farji-Brener, Alejandro Gustavo. (2005). The effect of abandoned leaf-cutting ant nests on plant assemblage composition in a tropical rainforest of Costa Rica. *Écoscience*, *12*(4), 554–560.

Fletcher, R. S., Everitt, J. H., & Drawe, L. (2007). *Detecting red harvester ant mounds with panchromatic QuickBird imagery*. *1*, 1–11. https://doi.org/10.1117/1.2830848

Folgarait, P. J. (1998). Ant biodiversity and its relationship to ecosystem functioning: A review. *Biodiversity and*

Conservation, *7*(9), 1221–1244. https://doi.org/10.1023/A:1008891901953

Frouz, J., Holec, M., & Kalčík, J. (2003). The effect of Lasius niger (Hymenoptera, Formicidae) ant nest on selected soil chemical properties. *Pedobiologia*, *47*(3), 205–212. https://doi.org/10.1078/0031-4056-00184

Garrettson, M., Stetzel, J., Halper, B. S., Hearn, D. J., Lucey, B. T., & McKone, M. J. (1998). Diversity and abundance of understorey plants on active and abandoned nests of leaf-cutting ants (Atta cephalotes) in a Costa Rican rain forest. *Journal of Tropical Biology*, *14*, 17–26.

Golichenkov, M. V., Maksimova, I. A., Zakalyukina, Y. V., Dymova, A. A., Churilina, A. E., & Kiryushin, A. V. (2019). Ants' nesting activity as a factor of changes in soil physical properties. *IOP Conference Series: Earth and Environmental Science*, *368*(1). https://doi.org/10.1088/1755-1315/368/1/012013

Goryunov, D. N. (2015). Nest-building in ants Formica exsecta (Hymenoptera, Formicidae). *Entomological Review*, *95*(8), 953–958. https://doi.org/10.1134/S0013873815080035

Green, L. R., Olson, J. K., & Davis, M. R. (1977). *Aerial Photographic Detection of Imported Fire Ant Mounds *. 43*(8), 1051–1057.

Hester, A. J., Mitchell, F. J. G., Gordon, I. J., & Baillie, G. J. (1996). Activity patterns and resource use by sheep and red deer grazing across a grass/heather boundary. *Journal of Zoology*, *240*(4), 609–620. https://doi.org/10.1111/j.1469-7998.1996.tb05311.x

Hölldobler, B., & Wilson, E. O. (1990). *The Ants* (1st ed.). Harvard University Press.

IUCN (International Union for Conservation of Nature). (2021). *Green List*.

Jouquet, P., Dauber, J., Lagerlöf, J., Lavelle, P., & Lepage, M. (2006). Soil invertebrates as ecosystem engineers: Intended and accidental effects on soil and feedback loops. *Applied Soil Ecology*, *32*(2), 153–164. https://doi.org/10.1016/j.apsoil.2005.07.004

Kadochová, Š., & Frouz, J. (2013). Thermoregulation strategies in ants in comparison to other social insects, with a focus on Formica rufa. *F1000Research*, *2*(May), 280. https://doi.org/10.12688/f1000research.2-280.v1

Kilgour, R. J. (2012). In pursuit of "normal": A review of the behaviour of cattle at pasture. *Applied Animal Behaviour Science*, *138*(1–2), 1–11. https://doi.org/10.1016/j.applanim.2011.12.002

Kilpeläinen, J., Finér, L., Niemelä, P., Domisch, T., Neuvonen, S., Ohashi, M., Risch, A. C., & Sundström, L. (2007). Carbon, nitrogen and phosphorus dynamics of ant mounds (Formica rufa group) in managed boreal forests of different successional stages. *Applied Soil Ecology*, *36*(2–3), 156–163. https://doi.org/10.1016/j.apsoil.2007.01.005

Kilpeläinen, Jouni, Punttila, P., Sundström, L., Niemelä, P., Kilpeläinen, J., Punttila, P., Sundström, L., Niemelä, P., & Finer, L. (2005). Finnish Zoological and Botanical Publishing Board Forest stand structure , site type and distribution of ant mounds in boreal forests in Finland in the 1950s Leena Finér Source : Annales Zoologici Fennici , Vol . 42 , No . 3 , The Role of Red Wood Ants in. *Annales Zoologici Fennici*, *42*(3), 243–258.

Klimetzek, D., Stăncioiu, P. T., Paraschiv, M., & Niță, M. D. (2021). Ecological monitoring with spy satellite images—the case of red wood ants in Romania. *Remote Sensing*, *13*(3), 1–22. https://doi.org/10.3390/rs13030520

Konečná, M., Blažek, P., Fibich, P., Lisner, A., Pech, P., & Lepš, J. (2021). Anthills as habitat islands in a sea of temperate pasture. *Biodiversity and Conservation*, *30*(4), 1081–1099. https://doi.org/10.1007/s10531-021-02134-6

Kümmerli, R., & Keller, L. (2007). Contrasting population genetic structure for workers and queens in the putatively unicolonial ant Formica exsecta. *Molecular Ecology*, *16*(21), 4493–4503. https://doi.org/10.1111/j.1365-294X.2007.03514.x

Kutter, H. (1977). Formicidae: Hymenoptera. In *Insecta Helvetica 6*. Schweizerische Entomologische Gesellschaft.

Kuznetsova, A., Brockhoff, P. B., & Christensen, R. H. B. (2017). {lmerTest} Package: Tests in Linear Mixed Effects Models. *Journal of Statistical Software*, *82*(13), 1–26. https://doi.org/doi = {10.18637/jss.v082.i13

Lal, R. (1988). Effects of macrofauna on soil properties in tropical ecosystems. *Agriculture, Ecosystems and Environment*, *24*(1–3), 101–116. https://doi.org/10.1016/0167-8809(88)90059-X

Lavelle, P., Decaëns, T., Aubert, M., Barot, S., Blouin, M., Bureau, F., Margerie, P., Mora, P., & Rossi, J. P. (2006). Soil invertebrates and ecosystem services. *European Journal of Soil Biology*, *42*(SUPPL. 1). https://doi.org/10.1016/j.ejsobi.2006.10.002

Lenth, R. V. (2021). *emmeans: Estimated Marginal Means, aka Least-Squares Means*. https://cran.r-project.org/package=emmeans

Leuzinger, E. (1999). *Das zeitlich-räumliche Nutzungsmuster der Rothirsche (Cervus elaphus L.) auf der subalpinen Weide Stabelchod im Schweizerischen Nationalpark*. University of Zurich.

Lobry de Bruyn, A. L., & Conacher, A. J. (1990). The role of termites and ants in soil modification: A review. *Australian Journal of Soil Research*, *28*(1), 55–93. https://doi.org/10.1071/SR9900055

MacMahon, J. A., Mull, J. F., & Crist, T. O. (2000). Harvester ants (Pogonomyrmex spp.): Their community and ecosystem influences. *Annual Review of Ecology and Systematics*, *31*, 265–291. https://doi.org/10.1146/annurev.ecolsys.31.1.265

Maggini, R., Guisan, A., & Cherix, D. (2002). A stratified approach for modeling the distribution of a threatened ant species in the Swiss National Park. *Biodiversity and Conservation*, *11*.

Markó, B., Czekes, Z., Eros, K., Csata, E., & Szász-Len, A. M. (2012). The largest polydomous system of Formica ants (Hymenoptera: Formicidae) in Europe discovered thus far in Romania. *North-Western Journal of Zoology*, *8*(2), 287–291.

MeteoSchweiz. (2021). *IDAWEB*.

Pamilo, P. (1991). Life span of queens in the ant Formica exsecta. *Insectes Sociaux*, *6*, 111–119.

Platner, C. (2006). *Ameisen als Schlüsseltiere in einem Grasland* (P. D. T. Frank (ed.)). Universitätsverlag Göttingen.

Prior, K. M., Robinson, J. M., Meadley Dunphy, S. A., & Frederickson, M. E. (2014). Mutualism between co-introduced species facilitates invasion and alters plant community structure. *Proceedings of the Royal Society B: Biological Sciences*, *282*(1800). https://doi.org/10.1098/rspb.2014.2846

R Core Team. (2021). *R: A language and environment for statistical computing.* R Foundation for Statistical Computing.

Risch, A. C., Jurgensen, M. F., Schütz, M., & Page- Dumroese, D. A. (2005). THE CONTRIBUTION OF RED WOOD ANTS TO SOIL C AND N POOLS AND CO 2 EMISSIONS IN SUBALPINE FORESTS. *Ecology*, *86*(2), 419–430.

Rossi, C., Kneubühler, M., Schütz, M., Schaepman, M. M., Haller, R. M., & Risch, A. C. (2021). Spatial resolution , spectral metrics and biomass are key aspects in estimating plant species richness from spectral diversity in species-rich grasslands. *Remote Sensing in Ecology and Conservation*, 1–18. https://doi.org/10.1002/rse2.244

RStudio Team. (2021). *RStudio: Integrated Development Environment for R*. RStudio, PBC. http://www.rstudio.com/

Sambraus, H. H., Brummer, H., van Putten, G., Schäfer, M., & Wennrich, G. (1978). *Nutztierethologie -Das Verhalten landwirtschaftlicher Nutztiere - Eine angewandte Verhaltenskunde für die Praxis*. Verlag Paul Parey.

Sasaki, Y. (2007). The truth of the F-measure. *Teach Tutor Mater*, 1–5. http://www.cs.odu.edu/~mukka/cs795sum09dm/Lecturenotes/Day3/F-measure-YS-26Oct07.pdf

Schmitz, O. J. (2009). Effects of predator functional diversity on grassland ecosystem function. *Ecology*, *90*(9), 2339–2345.

Schorta, A. (1988). Vez l'alp da Grimmels. Istorgia da las alps da Zernez. *Octopus*.

Schumacher, E. (2010). *The impact of ants on the aboveground and belowground ecological network - field studies in a grassland and experiments with microcosms*.

Schütz, M., Kretz, C., Dekoninck, L., Iravani, M., & Risch, A. C. (2008). Impact of Formica exsecta Nyl. on seed bank and vegetation patterns in a subalpine grassland ecosystem. *Journal of Applied Entomology*, *132*(4), 295–305. https://doi.org/10.1111/j.1439-0418.2008.01293.x

Schütz, Martin, & Risch, A. C. (2013). Beziehungsnetze auf Weiden: Kerbameisen und Hirsche als Ökosystemgestalter. In H. Haller, A. Eisenhut, & R. M. Haller (Eds.), *Atlas des Schweizerischen Nationalparks.* (pp. 194–195). Haupt.

Schütz, Martin, & Risch, A. C. (2014). Ergebnis aus hundert Jahren Sukzessionsforschung: Die Weide bleibt. In B. Baur & T. Scheurer (Eds.), *Wissen schaffen: 100 Jahre Forschung im Schweizerischen Nationalpark* (pp. 150–175). Haupt.

Schütz, Martin, Risch, A. C., Leuzinger, E., Krüsi, B. O., & Achermann, G. (2003). Impact of herbivory by red deer (Cervus elaphus L.) on patterns and processes in subalpine grasslands in the Swiss National Park. *Forest Ecology and Management*, *181*(1–2), 177–188. https://doi.org/10.1016/S0378-1127(03)00131-2

Seifert, B. (2000). A taxonomic revision of the ant subgenus Coptoformica Mueller, 1923 (Hymenoptera, Formicidae). In *Zoosystema-Paris*- (Vol. 22, Issue 3, pp. 517–568).

Seifert, B. (2018). *The Ants of Central and North Europe*. lutra Verlags – und Vertriebsgesellschaft Tauer.

Silva, P. S. D., Leal, I. R., Wirth, R., Melo, F. P. L., & Tabarelli, M. (2012). Leaf-cutting ants alter seedling assemblages across second-growth stands of Brazilian Atlantic forest. *Journal of Tropical Ecology*, *28*(4), 361–368. https://doi.org/10.1017/S0266467412000259

Snyder, S. R., Crist, T. O., & Friese, C. F. (2002). Variability in soil chemistry and arbuscular mycorrhizal fungi in harvester ant nests: The influence of topography, grazing and region. *Biology and Fertility of Soils*, *35*(6), 406–413. https://doi.org/10.1007/s00374-002-0487-z

Song, Y., Chen, F., & Liao, K. (2020). Comparison of UAV-based multispectral sensors for detection of Solenopsis invicta Nests. *IOP Conference Series: Earth and Environmental Science*, *569*(1). https://doi.org/10.1088/1755-1315/569/1/012051

Streitberger, M., & Fartmann, T. (2015). Vegetation and climate determine ant-mound occupancy by a declining herbivorous insect in grasslands. *Acta Oecologica*, *68*, 43–49. https://doi.org/10.1016/j.actao.2015.07.004

Strickland, M. S., Hawlena, D., Reese, A., Bradford, M. A., & Schmitz, O. J. (2013). Trophic cascade alters ecosystem carbon exchange. *Proceedings of the National Academy of Sciences of the United States of America*, *110*(27), 11035–11038. https://doi.org/10.1073/pnas.1305191110

Sudd, J. H., Douglas, J. M., Gaynard, T., Murray, D. M., & Stockdale, J. M. (1977). The distribution of wood-ants s (Formica lugubris Zetterstedt) in a northern English forest. *Ecological Entomology*, 301–313.

Tasser, E., Walde, J., Tappeiner, U., Teutsch, A., & Noggler, W. (2006). *Land-use changes and natural reforestation in the Eastern Central Alps*. *118*, 115–129. https://doi.org/10.1016/j.agee.2006.05.004

Vogt, J. T. (2004a). Detection of imported fire ant (Hymenoptera: Formicidae) mounds with satellite imagery. *Environmental Entomology*, *33*(6), 1718–1721. https://doi.org/10.1603/0046-225X-33.6.1718

Vogt, J. T. (2004b). Quantifying imported fire ant (Hymenoptera; Formicidae) mounds with airborne digital imagery. *Environmental Entomology*, *33*(4), 1045–1051. https://doi.org/10.1603/0046-225X-33.4.1045

Vogt, J. T., & Oliver, J. A. (2006). Distribution and size of imported fire ant (Hymenoptera: Formicidae) mounds in recently invaded ball-and-burlap nurseries in Tennessee. *Journal of Entomological Science*, *41*(4), 385–393. https://doi.org/10.18474/0749-8004-41.4.385

Vogt, J. T., & Wallet, B. (2008). Feasibility of using template-based and object-based automated detection methods for quantifying black and hybrid imported fire ant (Solenopsis invicta and S. invicta × richteri) mounds in aerial digital imagery. *Rangeland Journal*, *30*(3), 291–295. https://doi.org/10.1071/RJ08007

Vogt, J. T., Wallet, B., & Coy, S. (2008). Dynamic thermal structure of imported fire ant mounds. *Journal of Insect Science*, *8*(April). https://doi.org/10.1673/031.008.3101

Wagner, D., & Jones, J. B. (2006). The impact of harvester ants on decomposition, N mineralization, litter quality, and the availability of N to plants in the Mojave Desert. *Soil Biology and Biochemistry*, *38*(9), 2593–2601. https://doi.org/10.1016/j.soilbio.2006.02.024

Wang, S., Wang, H., Li, J., & Zhang, Z. (2017). Ants can exert a diverse effect on soil carbon and nitrogen pools in a Xishuangbanna tropical forest. *Soil Biology and Biochemistry*, *113*, 45–52. https://doi.org/10.1016/j.soilbio.2017.05.027

Westoby, M. J., Brasington, J., Glasser, N. F., Hambrey, M. J., & Reynolds, J. M. (2012). ' Structure-from-Motion ' photogrammetry : A low-cost , effective tool for geoscience applications. *Geomorphology*, *179*, 300–314. https://doi.org/10.1016/j.geomorph.2012.08.021

Wickham, H. (2016). *ggplot2: Elegant Graphics for Data Analysis*. Springer-Verlag.

Wiezik, M., Gallay, I., Wieziková, A., Čiliak, M., & Dovciak, M. (2017). Spatial structure of traditional land organization allows long-term persistence of large Formica exsecta supercolony in actively managed agricultural landscape. *Journal of Insect Conservation*, *21*(2), 257–266. https://doi.org/10.1007/s10841-017-9973-3

Wildi, O. (2002). Modelling succession from pasture to forest in time and space. *Community Ecology*, *3*(2), 181–189. https://doi.org/10.1556/ComEc.3.2002.2.5

Wills, B. D., & Landis, D. A. (2018). The role of ants in north temperate grasslands: a review. *Oecologia*, *186*(2), 323–338. https://doi.org/10.1007/s00442-017-4007-0

Wood, S. N. (2011). Fast stable restricted maximum likelihood and marginal likelihood estimation of semiparametric generalized linear models. *Journal of the Royal Statistical Society (B)*, *73*(1), 3–36.

Wu, H., Batzer, D. P., Yan, X., Lu, X., & Wu, D. (2013). Contributions of ant mounds to soil carbon and nitrogen pools in a marsh wetland of Northeastern China. *Applied Soil Ecology*, *70*, 9–15. https://doi.org/10.1016/j.apsoil.2013.04.004

Wu, H., Lu, X., Wu, D., & Yin, X. (2010). Biogenic structures of two ant species Formica sanguinea and Lasius

flavus altered soil C, N and P distribution in a meadow wetland of the Sanjiang Plain, China. *Applied Soil Ecology*, *46*(3), 321–328. https://doi.org/10.1016/j.apsoil.2010.10.011

Wylie, R., Oakey, J., & Williams, E. R. (2021). Alleles and algorithms: The role of genetic analyses and remote sensing technology in an ant eradication program. *NeoBiota*, *66*, 55–73. https://doi.org/10.3897/neobiota.66.64523

Appendix

A.1 Temperature curve and differences between ant hill and surroundings

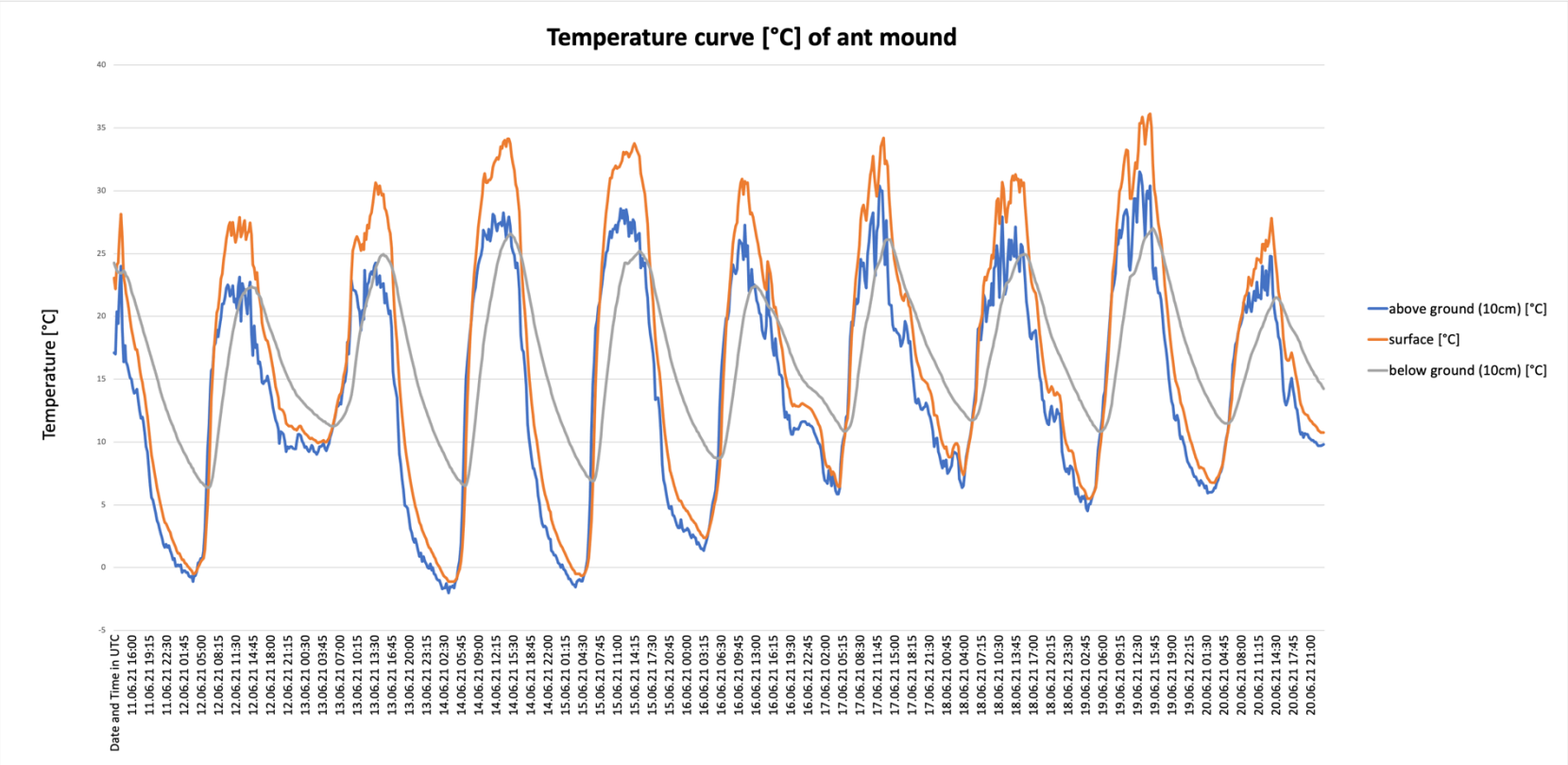

Appendix Figure 1: Temperature course at 10 cm above ground (blue), on the surface (orange) and at 10 cm below ground (grey) of a *F. exsecta* mound.

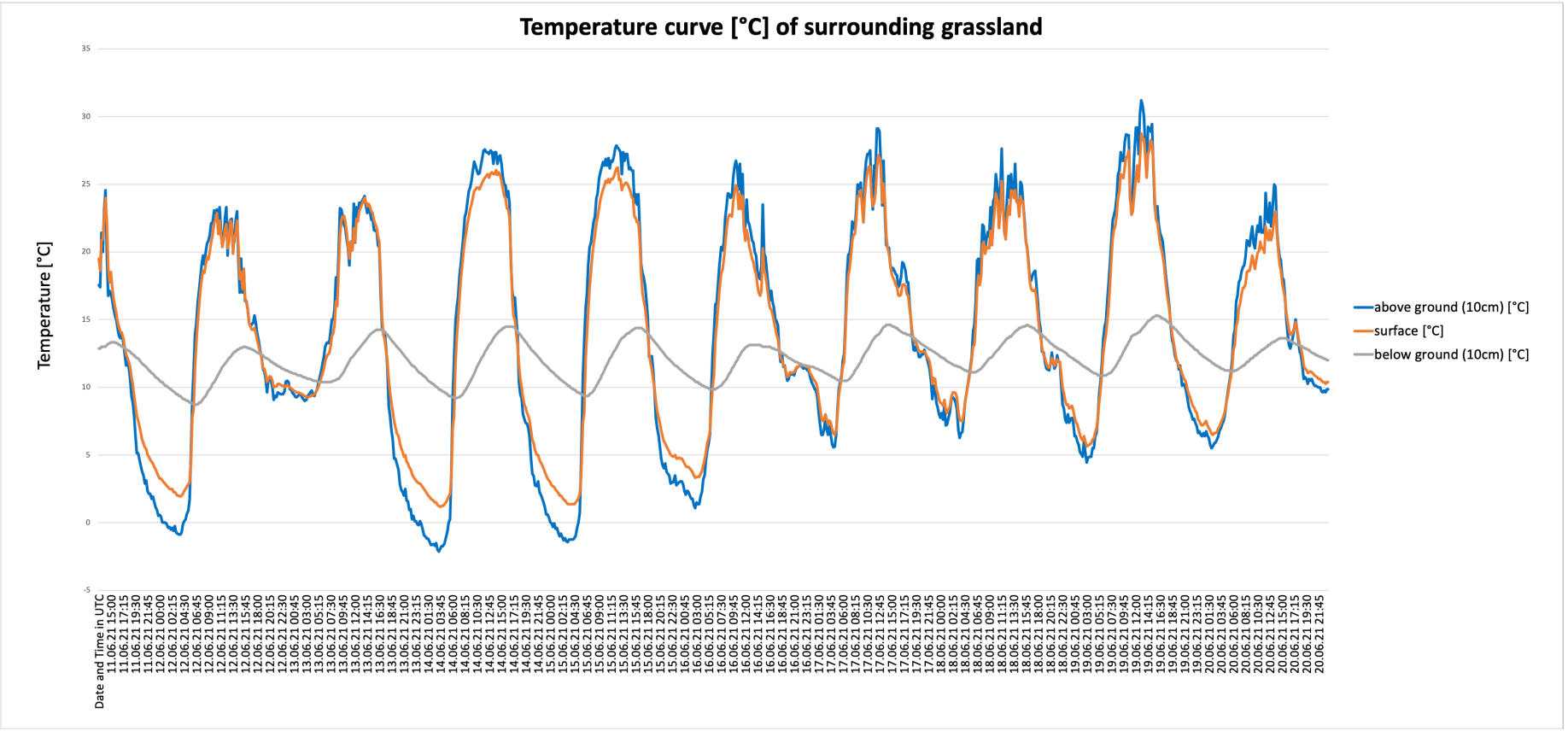

Appendix Figure 2: Temperature course at 10 cm above ground (blue), on the surface (orange) and at 10 cm below ground (grey) measured at 2 m distance of the *F. exsecta* mound.

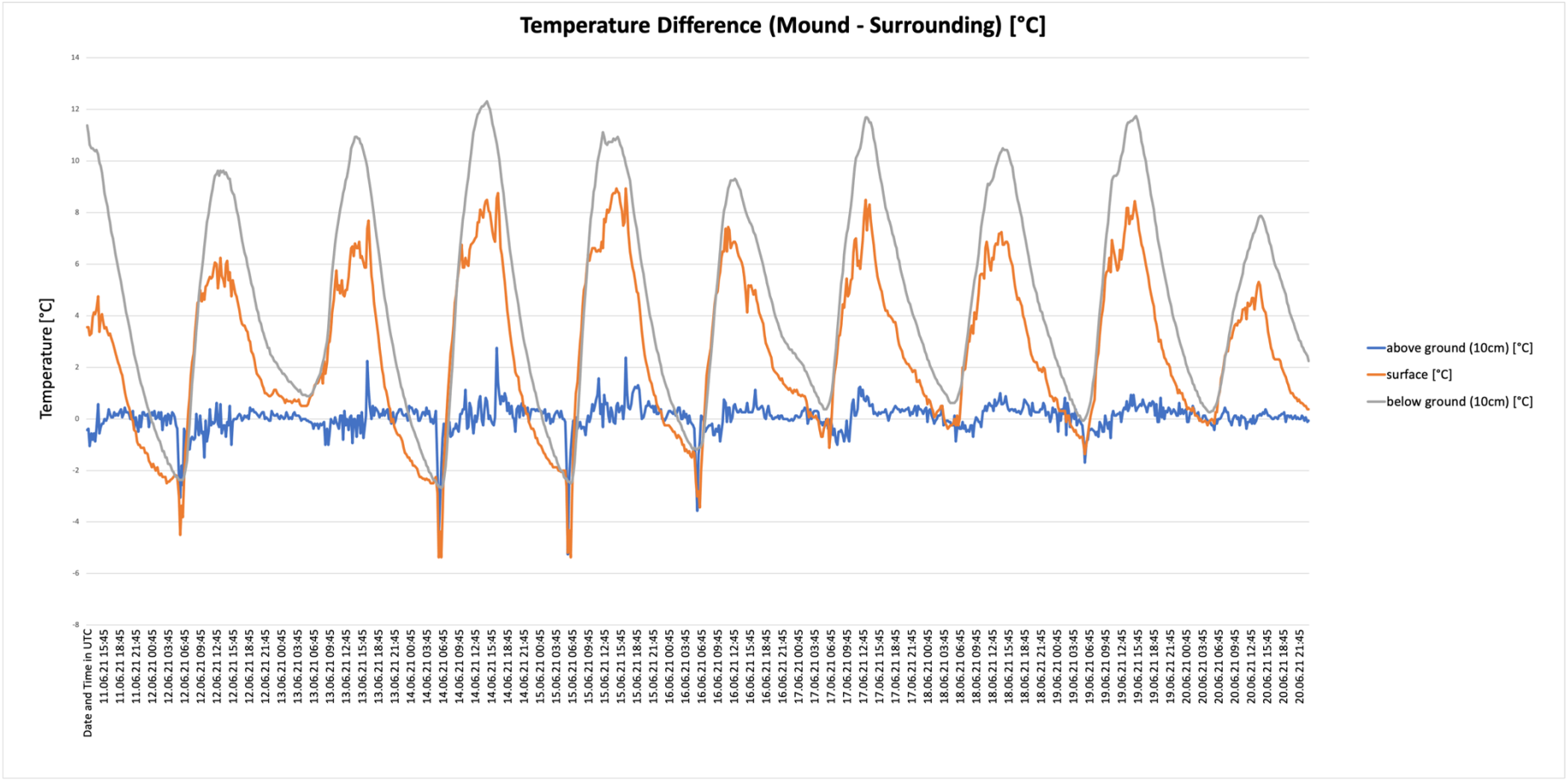

Appendix Figure 3: Temperature difference between logger located on *F. exsecta* mound and at 2 meters distance of the mound measured at 10 cm above ground (blue), on the surface (orange) and at 10 cm below ground (grey).

A.2 Quality Report

Quality Report

Generated with Pix4Dmapper version 4.5.6

Important: Click on the different icons for:

Help to analyze the results in the Quality Report

Additional information about the sections

Click here for additional tips to analyze the Quality Report

Summary

Project	thermal_60m
Processed	2021-06-30 17:06:31
Camera Model Name(s)	FLIRTau2640_0.0_640x512 (Grayscale)
Average Ground Sampling Distance (GSD)	6.23 cm / 2.45 in
Area Covered	0.138 km^2 / 13.8283 ha / 0.05 sq. mi. / 34.1882 acres

Quality Check

Images	median of 5948 keypoints per image	⚠
Dataset	539 out of 583 images calibrated (92%), 12 images disabled, 9 blocks	⚠
Camera Optimization	2.09% relative difference between initial and optimized internal camera parameters	✓
Matching	median of 2725.41 matches per calibrated image	✓
Georeferencing	yes, 26 GCPs (26 3D), mean RMS error = 0.705 m	✗

Preview

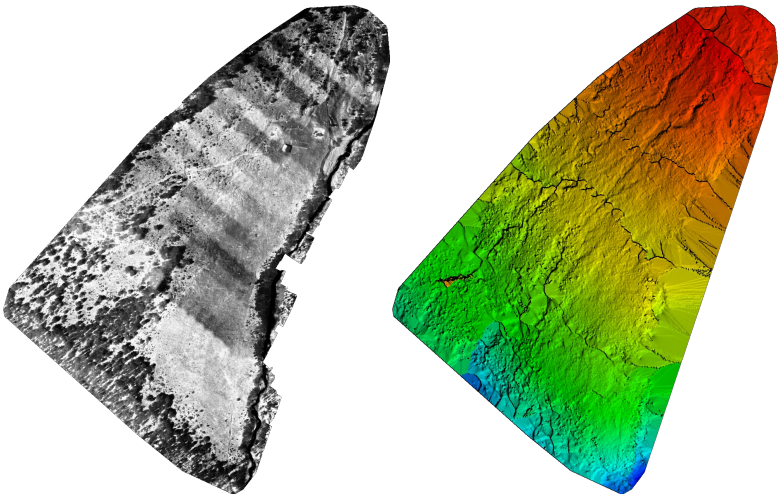

Figure 1: Orthomosaic and the corresponding sparse Digital Surface Model (DSM) before densification.

Calibration Details

Number of Calibrated Images	539 out of 595
Number of Geolocated Images	595 out of 595

Initial Image Positions

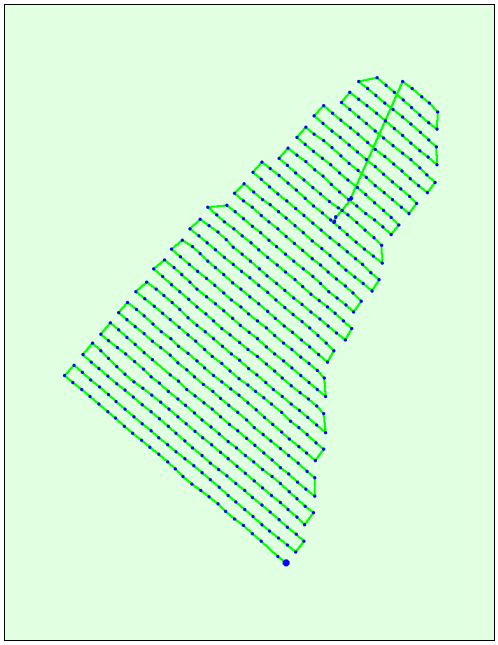

Figure 2: Top view of the initial image position. The green line follows the position of the images in time starting from the large blue dot.

Computed Image/GCPs/Manual Tie Points Positions

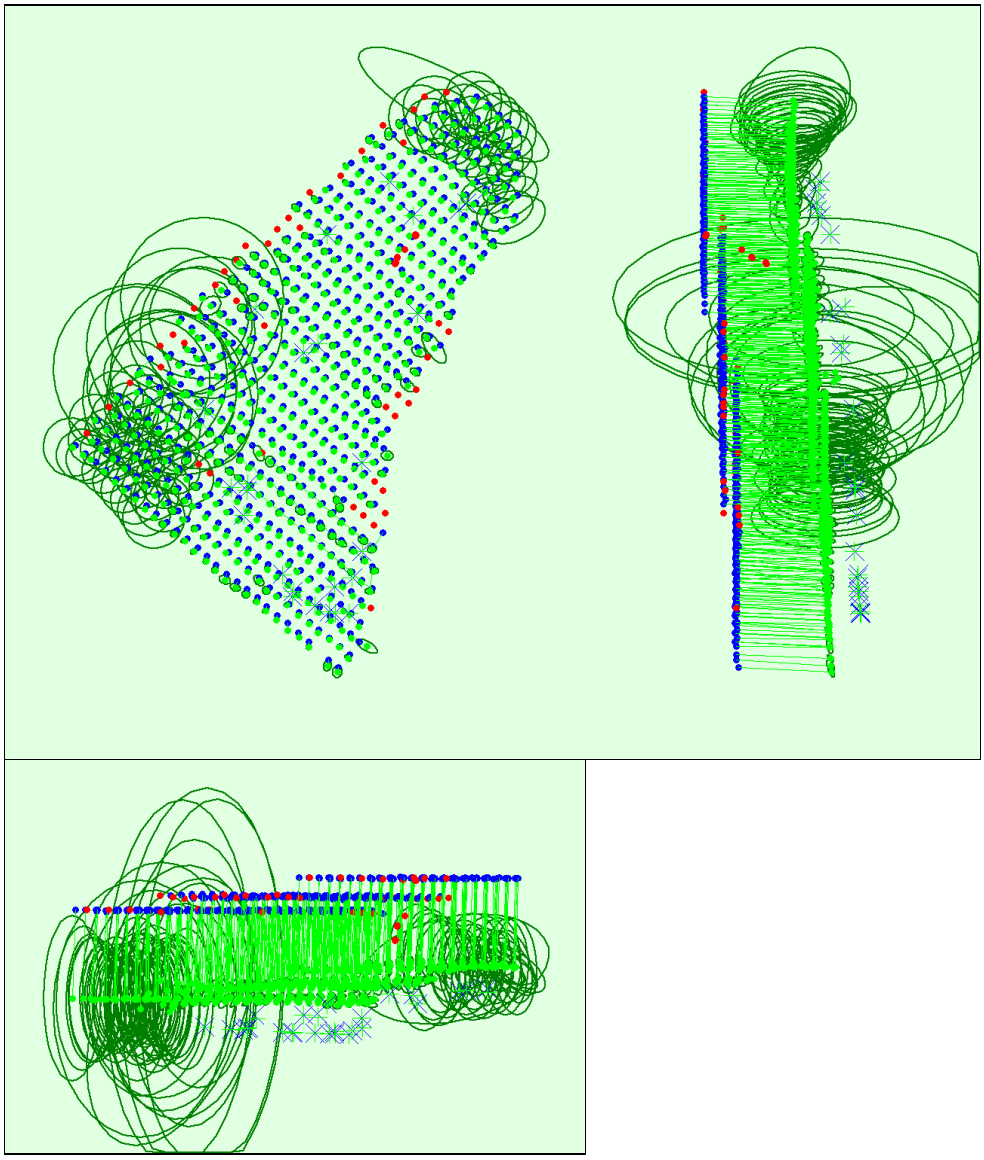

Uncertainty ellipses 10x magnified

Figure 3: Offset between initial (blue dots) and computed (green dots) image positions as well as the offset between the GCPs initial positions (blue crosses) and their computed positions (green crosses) in the top-view (XY plane), front-view (XZ plane), and side-view (YZ plane). Red dots indicate disabled or uncalibrated images. Dark green ellipses indicate the absolute position uncertainty of the bundle block adjustment result.

Absolute camera position and orientation uncertainties

	X [m]	Y [m]	Z [m]	Omega [degree]	Phi [degree]	Kappa [degree]
Mean	0.762	0.755	1.290	2.073	1.751	0.850
Sigma	1.322	1.304	2.657	5.906	5.095	2.841

Overlap

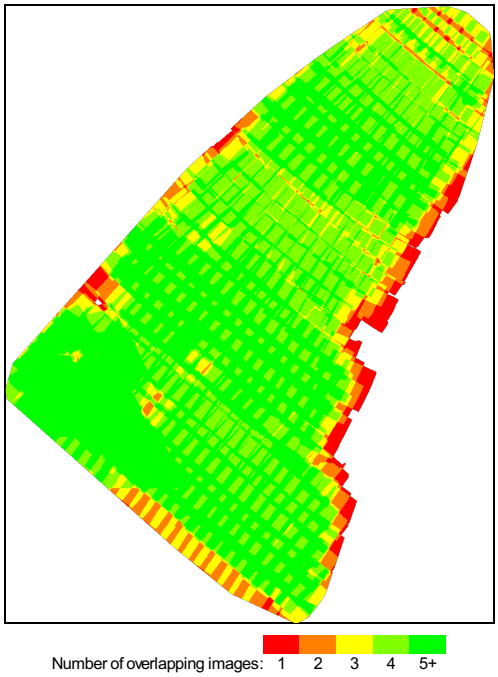

Figure 4: Number of overlapping images computed for each pixel of the orthomosaic.
Red and yellow areas indicate low overlap for which poor results may be generated. Green areas indicate an overlap of over 5 images for every pixel. Good quality results will be generated as long as the number of keypoint matches is also sufficient for these areas (see Figure 5 for keypoint matches).

Bundle Block Adjustment Details

Number of 2D Keypoint Observations for Bundle Block Adjustment	1414083
Number of 3D Points for Bundle Block Adjustment	516618
Mean Reprojection Error [pixels]	0.259

Internal Camera Parameters

FLIRTau2640_0.0_640x512 (Grayscale). Sensor Dimensions: 25.400 [mm] x 20.320 [mm]

EXIF ID: FLIRTau2640_0.0_640x512

	Focal Length	Principal Point x	Principal Point y	R1	R2	R3	T1	T2
Initial Values	503.937 [pixel] 20.000 [mm]	320.000 [pixel] 12.700 [mm]	256.000 [pixel] 10.160 [mm]	0.000	0.000	0.000	0.000	0.000
Optimized Values	514.477 [pixel] 20.418 [mm]	334.450 [pixel] 13.273 [mm]	207.283 [pixel] 8.227 [mm]	0.084	0.047	-0.027	-0.008	0.003
Uncertainties (Sigma)	2.150 [pixel] 0.085 [mm]	0.795 [pixel] 0.032 [mm]	0.717 [pixel] 0.028 [mm]	0.004	0.013	0.015	0.000	0.000

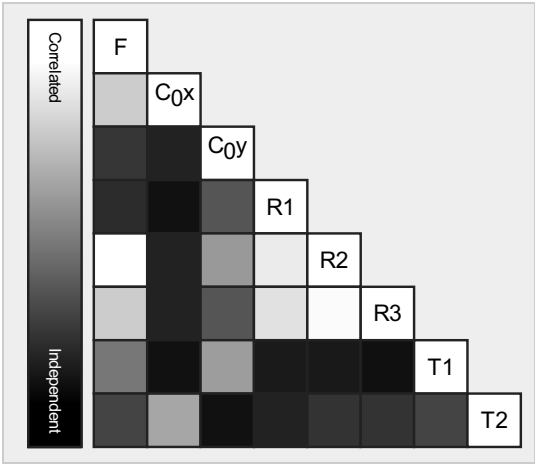

The correlation between camera internal parameters determined by the bundle adjustment. White indicates a full correlation between the parameters, ie. any change in one can be fully compensated by the other. Black indicates that the parameter is completely independent, and is not affected by other parameters.

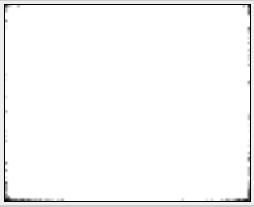

The number of Automatic Tie Points (ATPs) per pixel, averaged over all images of the camera model, is color coded between black and white. White indicates that, on average, more than 16 ATPs have been extracted at the pixel location. Black indicates that, on average, 0 ATPs have been extracted at the pixel location. Click on the image to the see the average direction and magnitude of the re-projection error for each pixel. Note that the vectors are scaled for better visualization. The scale bar indicates the magnitude of 1 pixel error.

2D Keypoints Table

	Number of 2D Keypoints per Image	Number of Matched 2D Keypoints per Image
Median	5948	2725
Min	3141	84
Max	9133	5692
Mean	6037	2624

3D Points from 2D Keypoint Matches

	Number of 3D Points Observed
In 2 Images	304244
In 3 Images	97858
In 4 Images	76818
In 5 Images	25399
In 6 Images	9089
In 7 Images	2523
In 8 Images	624
In 9 Images	63

2D Keypoint Matches

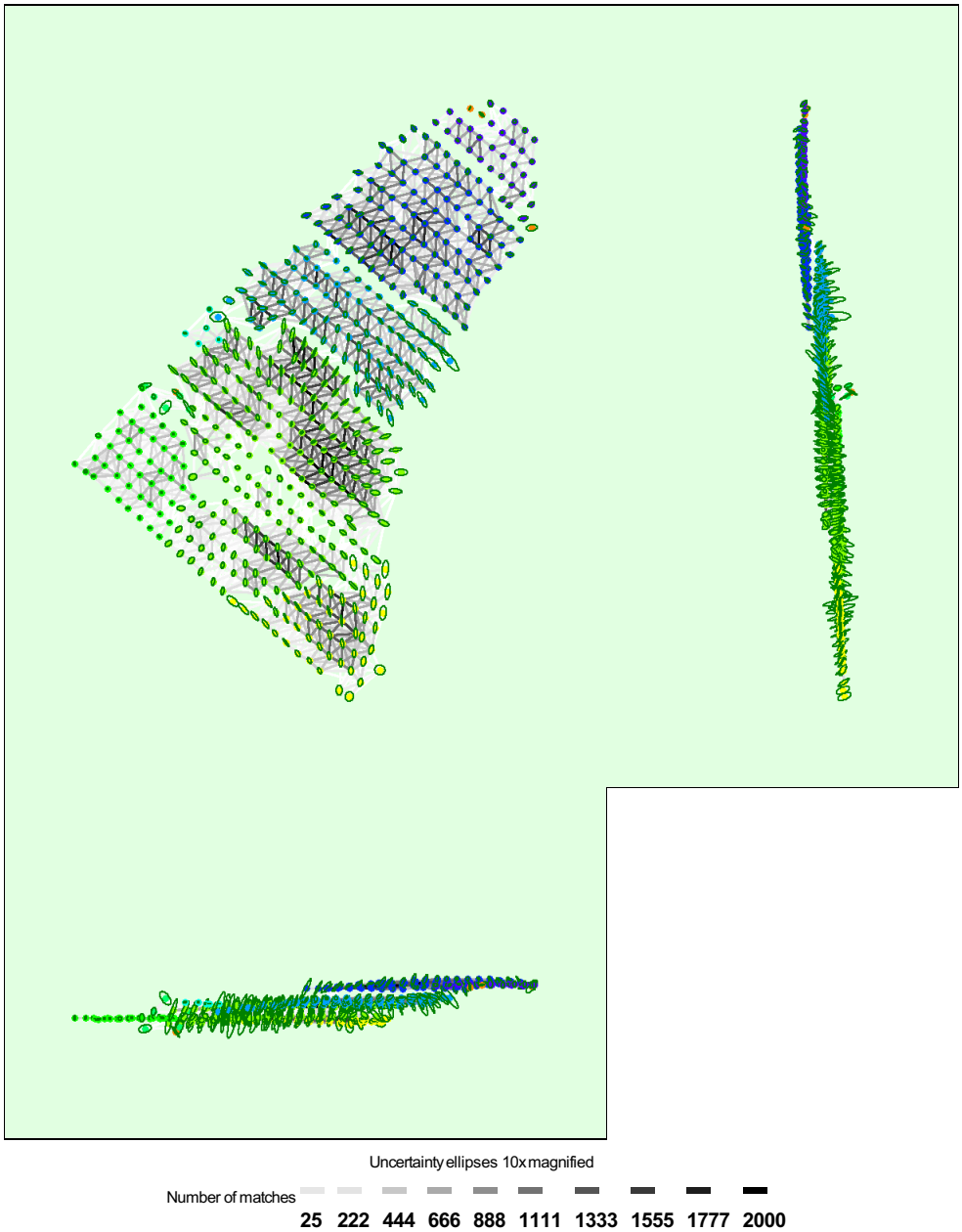

Figure 5: Computed image positions with links between matched images. The darkness of the links indicates the number of matched 2D keypoints between the images. Bright links indicate weak links and require manual tie points or more images. Dark green ellipses indicate the relative camera position uncertainty of the bundle block adjustment result.

Relative camera position and orientation uncertainties

	X[m]	Y[m]	Z[m]	Omega [degree]	Phi [degree]	Kappa [degree]
Mean	0.252	0.307	0.423	0.579	0.602	0.142
Sigma	0.134	0.179	0.316	0.357	0.353	0.198

Geolocation Details

Ground Control Points

GCP Name	Accuracy XY/Z [m]	Error X [m]	Error Y [m]	Error Z [m]	Projection Error [pixel]	Verified/Marked
pp01 (3D)	0.020/ 0.020	0.144	-0.025	0.028	0.924	3 / 3
pp02 (3D)	0.020/ 0.020	0.009	-0.036	-0.018	0.307	6 / 6
pp03 (3D)	0.020/ 0.020	0.058	0.025	0.044	0.636	4 / 4
pp04 (3D)	0.020/ 0.020	-0.041	0.068	0.012	0.775	5 / 5
pp05 (3D)	0.020/ 0.020	0.000	-0.000	0.000	0.965	4 / 4
pp06 (3D)	0.020/ 0.020	-0.155	0.673	3.477	12.956	5 / 5
pp07 (3D)	0.020/ 0.020	0.160	-0.001	-0.005	0.720	4 / 4
pp08 (3D)	0.020/ 0.020	-0.481	-0.639	0.996	4.454	4 / 4
sta_am_1 (3D)	0.020/ 0.020	-0.101	0.036	0.014	0.769	4 / 4
sta_am_2 (3D)	0.020/ 0.020	0.067	0.028	-0.099	0.399	4 / 4
sta_am_5 (3D)	0.020/ 0.020	-0.089	0.052	0.173	0.860	4 / 4
sta_am_12 (3D)	0.020/ 0.020	0.351	0.361	0.230	0.727	4 / 4
sta_am_15 (3D)	0.020/ 0.020	-0.131	-0.329	0.263	0.466	4 / 4
sta_am_25 (3D)	0.020/ 0.020	0.085	0.578	-0.554	11.468	4 / 4
sta_am_47 (3D)	0.020/ 0.020	-0.165	0.081	0.002	0.848	4 / 4
sta_am_59 (3D)	0.020/ 0.020	0.040	0.031	0.067	0.574	3 / 3
sta_am_66 (3D)	0.020/ 0.020	0.126	-0.010	0.074	1.587	4 / 4
sta_am_72 (3D)	0.020/ 0.020	-0.018	-0.177	-0.110	1.080	4 / 4
sta_am_82 (3D)	0.020/ 0.020	-0.065	0.055	-0.111	1.130	5 / 5
sta_am_102 (3D)	0.020/ 0.020	0.098	-0.027	0.059	0.797	4 / 4
sta_am_123 (3D)	0.020/ 0.020	-0.599	0.229	-0.615	15.412	4 / 4
sta_am_152 (3D)	0.020/ 0.020	-1.552	-1.863	4.076	1.009	4 / 4
sta_am_174 (3D)	0.020/ 0.020	-0.211	-0.124	0.035	0.721	4 / 4
sta_am_177 (3D)	0.020/ 0.020	0.010	0.065	0.060	0.450	3 / 3
sta_am_179 (3D)	0.020/ 0.020	0.335	0.070	-0.102	0.990	4 / 4
sta_am_187 (3D)	0.020/ 0.020	-0.993	-1.069	3.829	20.267	4 / 4
Mean [m]		-0.119980	-0.074915	0.454711		
Sigma [m]		0.395802	0.481720	1.238539		
RMS Error [m]		0.413587	0.487510	1.319371		

Localisation accuracy per GCP and mean errors in the three coordinate directions. The last column counts the number of calibrated images where the GCP has been automatically verified vs. manually marked.

Absolute Geolocation Variance

Min Error [m]	Max Error [m]	Geolocation Error X [%]	Geolocation Error Y [%]	Geolocation Error Z [%]
-	-15.00	0.37	0.00	0.19
-15.00	-12.00	2.60	0.00	0.00
-12.00	-9.00	0.93	5.19	0.00
-9.00	-6.00	0.37	1.48	1.48
-6.00	-3.00	3.15	2.97	12.24
-3.00	0.00	45.45	38.03	35.99
0.00	3.00	37.48	42.49	35.62
3.00	6.00	2.78	5.19	13.17
6.00	9.00	1.67	0.19	0.93
9.00	12.00	5.01	3.90	0.19
12.00	15.00	0.19	0.37	0.19
15.00	-	0.00	0.19	0.00
Mean [m]		2.546834	2.341147	93.260039
Sigma [m]		3.942460	3.865217	3.017224

RMS Error [m]	4.693544	4.518946	93.308834

Min Error and Max Error represent geolocation error intervals between -1.5 and 1.5 times the maximum accuracy of all the images. Columns X, Y, Z show the percentage of images with geolocation errors within the predefined error intervals. The geolocation error is the difference between the initial and computed image positions. Note that the image geolocation errors do not correspond to the accuracy of the observed 3D points.

Geolocation Bias	X	Y	Z
Translation [m]	2.546834	2.341147	93.260039

Bias between image initial and computed geolocation given in output coordinate system.

Relative Geolocation Variance

Relative Geolocation Error	Images X [%]	Images Y [%]	Images Z [%]
[-1.00, 1.00]	88.31	88.31	99.44
[-2.00, 2.00]	93.69	94.99	100.00
[-3.00, 3.00]	99.63	99.81	100.00
Mean of Geolocation Accuracy [m]	5.000000	5.000000	10.000000
Sigma of Geolocation Accuracy [m]	0.000000	0.000000	0.000000

Images X, Y, Z represent the percentage of images with a relative geolocation error in X, Y, Z.

Initial Processing Details

System Information

Hardware	CPU: Intel(R) Xeon(R) CPU E5-2650 v4 @ 2.20GHz RAM: 128GB GPU: Microsoft Remote Display Adapter (Driver: unknown), Microsoft Remote Display Adapter (Driver: unknown), Microsoft Remote Display Adapter (Driver: unknown), Microsoft Remote Display Adapter (Driver: unknown), Microsoft Remote Display Adapter (Driver: unknown), Microsoft Remote Display Adapter (Driver: unknown), Microsoft Remote Display Adapter (Driver: unknown), Microsoft Remote Display Adapter (Driver: unknown), Microsoft Remote Display Adapter (Driver: unknown), Microsoft Remote Display Adapter (Driver: unknown), Microsoft Remote Display Adapter (Driver: unknown), Microsoft Remote Display Adapter (Driver: unknown), Microsoft Remote Display Adapter (Driver: unknown), Microsoft Remote Display Adapter (Driver: unknown), Microsoft Remote Display Adapter (Driver: unknown), Microsoft Remote Display Adapter (Driver: unknown), Microsoft Remote Display Adapter (Driver: unknown)
Operating System	Windows 10 Pro, 64-bit

Coordinate Systems

Image Coordinate System	WGS 84 (EGM96 Geoid)
Ground Control Point (GCP) Coordinate System	CH1903+ / LV95 (2D)
Output Coordinate System	CH1903+ / LV95 (2D)

Processing Options

Detected Template	No Template Available
Keypoints Image Scale	Custom, Image Scale: 2
Advanced: Matching Image Pairs	Aerial Grid or Corridor
Advanced: Matching Strategy	Use Geometrically Verified Matching: yes
Advanced: Keypoint Extraction	Targeted Number of Keypoints: Automatic
Advanced: Calibration	Calibration Method: Alternative Internal Parameters Optimization: All prior External Parameters Optimization: All Rematch: Auto, no

Point Cloud Densification details

Processing Options

Image Scale	multiscale, 1 (Original image size, Slow)
Point Density	High (Slow)
Minimum Number of Matches	3
3D Textured Mesh Generation	no
LOD	Generated: no
Advanced: Image Groups	Grayscale
Advanced: Use Processing Area	yes
Advanced: Use Annotations	yes
Time for Point Cloud Densification	04m:29s
Time for Point Cloud Classification	NA
Time for 3D Textured Mesh Generation	NA

Results

Number of Generated Tiles	1
Number of 3D Densified Points	21152583
Average Density (per m^3)	161.33

DSM, Orthomosaic and Index Details

Processing Options

DSM and Orthomosaic Resolution	1 x GSD (6.23 [cm/pixel])
DSM Filters	Noise Filtering: yes Surface Smoothing: yes, Type: Sharp
Orthomosaic	Generated: yes Merge Tiles: yes GeoTIFF Without Transparency: no Google Maps Tiles and KML: no
Index Calculator: Reflectance Map	Generated: yes Resolution: 1 x GSD (6.23 [cm/pixel]) Merge Tiles: no
Time for DSM Generation	00s
Time for Orthomosaic Generation	03m:37s
Time for DTM Generation	00s
Time for Contour Lines Generation	00s
Time for Reflectance Map Generation	03m:46s
Time for Index Map Generation	00s

A.3 Optimized Hot Spot Analysis

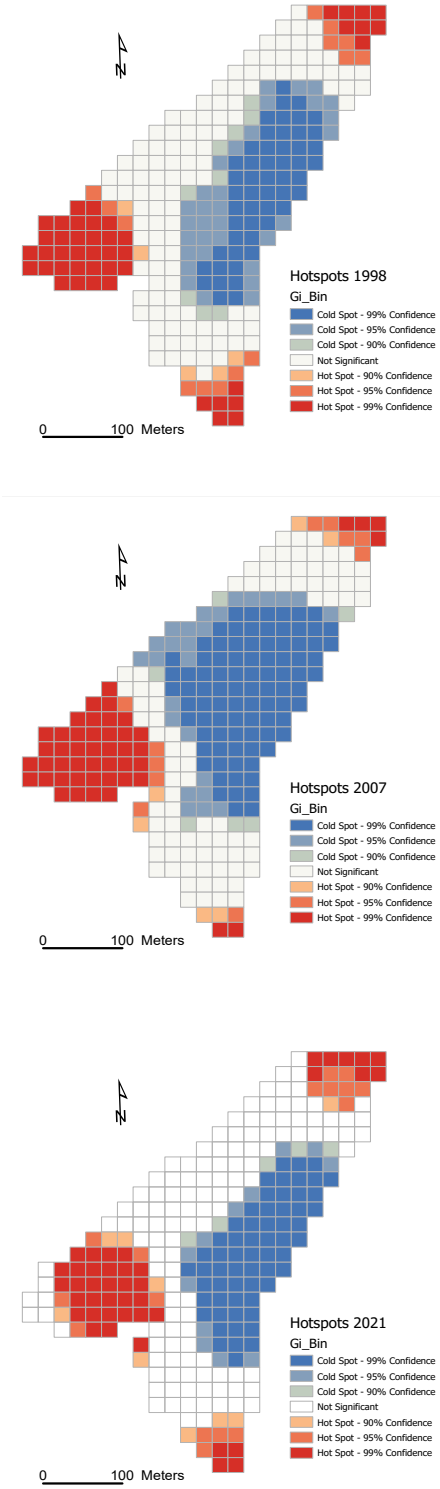

Appendix Figure 4: Optimized Hotspot Analysis (Spatial Statistics Toolbox; ArcGIS Pro 2.7.0) for the year 1998 (A), 2007 (B) and 2021 (C). This tool identifies statistically significant spatial clusters with high values (hot spots; red) and with low values (cold spots; blue) of mound counts. The size of the hot and cold spots varies over the years but the location remains relatively stable.

A.4 Diameter distribution of ant mounds on Alp Stabelchod

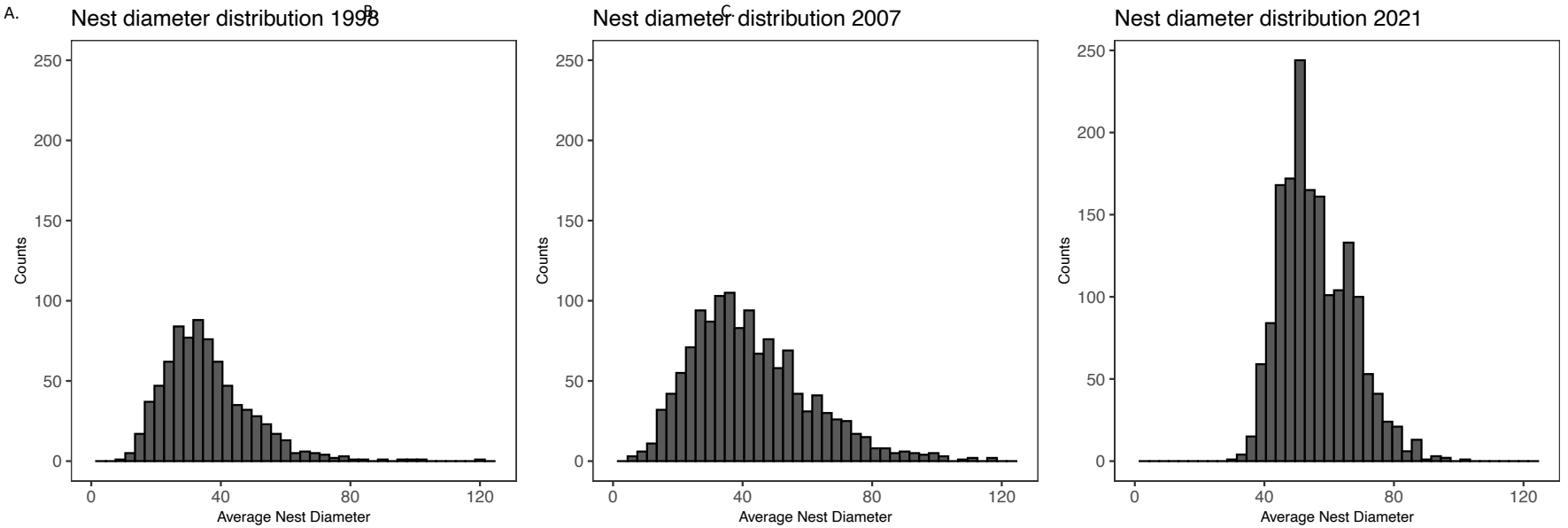

Appendix Figure 5: *F. exsecta* mounds counted (y-axis) in nest diameter classes (x-axis) in the years 1998 (A.), 2007 (B.) and 2021 (C.)